MASTERARBEIT | MASTER'S THESIS

Titel | Title

CYP27A1 driven metabolic control in macrophages regulates the tumor microenvironment

verfasst von | submitted by

Lovro Davidovski BSc

angestrebter akademischer Grad | in partial fulfilment of the requirements for the degree of

Master of Science (MSc)

Wien | Vienna, 2025

Studienkennzahl lt. Studienblatt | Degree programme code as it appears on the student record sheet:	UA 066 830
Studienrichtung lt. Studienblatt | Degree programme as it appears on the student record sheet:	Masterstudium Molecular Microbiology, Microbial Ecology and Immunobiology
Betreut von | Supervisor:	Assoc. Prof. Priv. Doz. Mag. Dr. Thomas Weichhart

TABLE OF CONTENTS

1. Introduction

1.1 Cancer and Metabolism, Two Sides of the Same Coin

Cancer is currently one of the leading causes of death worldwide, with the World Health Organization reporting it as the second most common cause of death in 2020, accounting for approximately 10 million deaths (Sung et al., 2021). Despite extensive research and decades of accumulated data, our understanding of this disease remains incomplete. It is essential to recognize cancer not merely as a conventional disease but as a complex phenomenon involving sequential alterations at the molecular, cellular, tissue, and organ levels, which impact the entire physiology of the organism (Upadhyay, 2020).

Over the decades, numerous theories have been proposed to explain the origins of cancer. Among the most prominent are (**1**) the mutation theory, which argues that cancer arises from the accumulation of genetic mutations in the genome (Brücher & Jamal, 2016); (**2**) the chromosomal imbalance theory, which suggests that cancer develops due to abnormal chromosomal structures, which lead to genomic instability (Duesberg et al., 2011); (**3**) the mitochondrial dysfunction theory, which proposes that cancer initiation is triggered by impaired mitochondrial function, resulting in energy deficits that disrupt cellular processes (Seyfried, 2015); and (**4**) the environment and matter theory, which proposes that cancer results from changes in the cellular microenvironment, influenced by external factors such as hormones and pH levels (Baker, 2014). Each theory has its strengths, but none is sufficient to explain the cause and progression of cancer exclusively.

In this context, Hanselmann and Welter propose an overarching framework that combines these different models, suggesting that cancer can be understood as a disease of information, energy, and matter. Energy loss (e.g., through impaired mitochondrial function), information disturbance (e.g., through mutations or aneuploidy), or changes in matter (e.g., through microenvironmental alterations or toxic agents) can irreversibly disrupt molecular mechanisms, leading to increased cellular entropy. This leads to a thermodynamically stable but biologically imbalanced state. Cells either die or persist in a metastable state, initiating an adaptive process that can generate a spectrum of disordered cells, potentially leading to cancer (Hanselmann & Welter, 2016).

In order to maintain a stable internal environment, cells must absorb nutrients such as amino acids, lipids, carbohydrates, and electrolytes from their surroundings. Under normal

physiological conditions, the cell's surroundings are regulated to meet its needs. However, significant environmental changes or disruptions in nutrient supply can have profound effects. Studies of cancerous tissues reveal that they are often surrounded by substantial changes in the tumor microenvironment (TME) (Ryan et al., 2020; Reina-Campos et al., 2021; de Visser & Joyce, 2023). Conceptualizing cancer as a multifaceted disease without a single cause, and understanding the accompanying TME changes, can help improve current treatment strategies and guide future therapeutic approaches.

1.2 Tumor Microenvironment

The TME consists of cancerous and non-cancerous cells, as well as their respective components, all present within the tumor. While oncogenic mutations are undoubtedly necessary for cancer, they alone are not sufficient for its initiation and progression. The complexity of solid tumors becomes self-evident upon microscopic analysis, revealing the TME as a highly organized environment, in which cancer cells are surrounded by diverse non-malignant cell types embedded within a vascularized extracellular matrix (de Visser & Joyce, 2023).

The formation of the TME is fundamentally driven by reciprocal communication between cancer cells and host cells, which orchestrates a tumor supportive environment. This is achieved in two major ways: through remodeling of the extracellular matrix and vasculature, as well as through the recruitment and reprogramming of host cells (de Visser & Joyce, 2023). Reprogrammed cells can aid tumor progression via direct cell-cell interactions, such as those observed in PD-L1/PD-1 interactions. Tumor-associated myeloid cells, as well as cancer cells, overexpress the immune checkpoint inhibitor PD-L1, which binds PD-1 on adaptive immune cells, thereby inhibiting their immune clearance and surveillance functions (Sharma et al., 2021). In fact, treatment with anti-PD-1 or anti-PD-L1 antibodies has become the standard approach for many cancers (Sharma et al., 2021). Additionally, paracrine signaling through the release of various cytokines, chemokines, proteases, and growth factors plays a critical role in reshaping the host response to tumor progression. These molecules are released by multiple cell types in the TME, mostly in response to cancer-intrinsic features or cellular stress and they exert both direct and indirect effects on target cells via intracellular signaling or extracellular matrix (ECM) remodeling (Ryan et al., 2020; Reina-Campos et al., 2021; de Visser & Joyce, 2023).

Major non-cancerous cellular cohorts that comprise the TME in solid cancers fall into four categories, each with distinct adaptations and roles. First, vascular cells, such as endothelial cells, form a single layer lining the interior of blood vessels and regulate the flux of nutrients, oxygen, and proteins into the TME. Endothelial cells in the TME often express fewer adhesion molecules, which impairs barrier function and is associated with increased expression of inhibitory immune checkpoint molecules, thereby contributing to immunosuppression. (Amersfoort et al., 2022). Second, stromal cells such as cancer-associated fibroblasts, synthesize and remodel the ECM, thereby influencing cancer- and immune cell behavior (Kalluri, 2016). Third, adaptive immune cells, for example intratumoral $CD8^+$ cytotoxic T cells, often lose their tumor suppressive effector functions and exhibit an exhaustion phenotype in the TME (Philip & Schietinger, 2022). Finally, innate immune cells, such as tumor-associated macrophages (TAMs), which represent a highly plastic cell population, fulfilling both pro-tumorigenic functions, like promoting angiogenesis, immunosuppression, and advancing metastasis, but also anti-tumorigenic functions, like tumor clearance via phagocytosis (Ryan et al., 2020).

Understanding the intricate interplay among all the cellular constituents of the TME is challenging due to their complex cross-interactions. However, by isolating and focusing on the contributions of specific cell types, the TME can be studied more effectively. Therefore, in this thesis, I primarily focus on the regulation of the TME by macrophages.

1.3 Cancer Immunometabolismus

Cancer is highly diverse, so it is not surprising that its metabolism often exhibits atypical characteristics. The mechanisms through which these metabolic changes benefit cancer are complex and have attracted considerable scientific interest, as they represent a significant barrier to effective cancer treatment (Dang et al., 2024). The first instance describing cancer-specific reprogramming of localized metabolism was the discovery of the Warburg effect by its namesake, Otto Warburg, and his colleagues in the 1920s (Warburg et al., 1924; Dang et al., 2024). Many solid tumors exhibit the Warburg effect, in which mitochondrial respiration diminishes, and anaerobic glycolysis takes over to produce ATP, a highly inefficient process compared to oxidative phosphorylation, generating only about 1/16 of the ATP (Vercellino & Sazanov, 2021). While this energetically inefficient phenotype might be expected to limit tumor growth when glucose is depleted, it instead establishes a unique metabolic milieu in the TME, characterized by low glucose levels, elevated lactate concentrations, and a decreased overall pH (Singer et al., 2018). Today, it is understood that such conditions lead to nutrient deprivation of

surrounding immune cells, thereby metabolically starving them in addition to impairing T cell receptor (TCR) signaling under acidic conditions (Dang et al., 2024; Rahman et al., 2024).

Furthermore, tumors have been found to dysregulate additional metabolic pathways while simultaneously enhancing their metabolic flexibility, leading to compromised immune clearance and tumor progression. For instance, dysregulated processes in the TME, such as ASCT2 mediated glutamine uptake, impair T cell activation and differentiation. Such dysregulation results in attenuated inflammatory responses that promote immune evasion (Nakaya et al., 2014). Abnormal glucose metabolism is involved in the activation of the methyltransferase NSUN2, leading to suppression of cGAS/STING signaling, thereby facilitating tumorigenesis and resistance to anti-PD-L1 immunotherapy (Chen et al., 2023). Additionally, sterol regulatory element-binding protein (SREBP)-dependent de novo lipid synthesis and metabolic signaling in regulatory T cells (Tregs) diminishes anti-tumor immune responses in the TME by promoting their functional maturation (Lim et al., 2021). Modulation of cholesterol metabolism and trafficking via lipid droplets (LDs) supplies resources for rapid cancer growth and provides a mechanism to eliminate reactive oxygen species, thereby reducing cellular stress in tumor cells (Jin et al., 2023). Furthermore, the differentiation and effector function of many immune cells, such as T cells (Reina-Campos et al., 2021) and macrophages (Ryan et al., 2020), are regulated by local metabolites and cancers have been shown to directly compete with immune cells for nutrients, leading to dysregulated immune cell functions (Dang et al., 2024).

Taken together, these findings illustrate how cancer can exploit energy consumption and metabolic reprogramming to foster tolerogenic immune cell populations within the TME. In turn, these tolerogenic populations promote immune tolerance, ultimately resulting in inefficient cancer clearance. This issue is particularly problematic in solid tumors, where conventional immune checkpoint blockade immunotherapies achieve response rates rarely exceeding 40% (Hargadon et al., 2018). Understanding the intricate interplay between solid cancers and immunometabolism is thus considered a promising strategy for enhancing immune cell fitness in the TME and paving the way for effective combination therapies (Guerra et al., 2020).

1.4 Macrophages

Macrophages were first described by the Nobel Prize winner and father of cellular immunology, Elie Metchnikoff, in the late 19th century. Research interest in macrophages has been rising in

recent years, as their involvement in a plethora of bodily functions has become increasingly evident (Cavaillon, 2011). They are myeloid cells that are part of the innate immune system and fulfill functions in various cellular and organ-specific contexts (Lesbats et al., 2025). Their most prominent function is phagocytosis, a cellular process that eliminates extracellular matter through internalization and degradation. In order to discriminate between self and microbial or infectious agents, a restricted number of phagocytic and scavenging receptors is expressed by macrophages (Aderem & Underhill, 1999). A notable example is the cluster of differentiation (CD) 206, also known as the mannose receptor, which recognizes conserved glycoproteins with terminal mannose, fucose, or N-acetyl-glucosamine on bacteria and mediates phagocytosis (Martinez-Pomares, 2012). Phagocytosed bacteria can thereafter be recycled into building blocks for protein synthesis and used as fuel for mitochondrial oxidative phosphorylation, indicating that macrophages can partially sustain themselves through phagocytosis (Lesbats et al., 2025). Macrophages also play a crucial role in wound healing and tissue repair. During the initial phase, they clear cellular debris and modulate cytokine production to facilitate the transition away from an inflammatory state (Oishi & Manabe, 2018). Additionally, macrophages promote the formation of the ECM, providing a scaffold for tissue regeneration, and produce metalloproteinases (MMPs) to regulate fibrosis (Oishi & Manabe, 2018). Furthermore, macrophages contribute to angiogenesis and vascular remodeling by releasing pro-angiogenic growth factors, such as vascular endothelial growth factor (VEGF)-β (Zordan et al., 2014).

However, it is important to note that not all macrophages are identical. Different populations of macrophages are present in virtually every organ of the body, playing active roles in maintaining tissue homeostasis and coordinating tissue-specific cellular metabolism (Li et al., 2023). In broad terms, the origin and function of macrophages can be considered along three axes:

(1) the tissue-specific axis: Different organs exhibit distinct macrophage populations, such as Langerhans cells in the skin or Kupffer cells in the liver. A prominent explanation is provided by the “Niche Theory” proposed by Guilliams, which posits that tissue-resident macrophages are maintained in specialized microenvironments, or “niches,” throughout the body. These niches supply trophic factors like colony-stimulating factors (CSFs) and cytokines such as IL-34, supporting macrophage self-renewal and imprinting tissue-specific identities through transcriptional and epigenetic modifications. This reciprocal system optimizes macrophages for their niche and ensures they maintain homeostatic functions within the tissue (Lavin et al., 2014; Guilliams et al., 2020).

(2) The ontogenetic axis: Macrophages can be classified based on cellular ontogeny. Prenatal macrophages, derived from successive waves of embryonic hematopoiesis in the yolk sac or aorta-gonad-mesonephros, seed various tissues (Ginhoux et al., 2010; Varol et al., 2015). In steady-state conditions, these macrophages often form a pool of tissue-resident macrophages with self-renewing capacity (Hashimoto et al., 2013). In contrast, monocyte-derived macrophages in adults differentiate from hematopoietic stem cells and replenish diminishing or unstable macrophage subpopulations, often strongly pronounced in immunologically active tissue such as in the lamina propria of the colon (Mildner, 2013).

(3) The polarization axis: Most importantly for this thesis, macrophage differentiation is strongly influenced by pathological conditions and resulting immunological signaling. Macrophage polarization, i.e., the alteration of their phenotype upon activation, is not static process but instead highly variable in space and time (Murray, 2017). Macrophages exhibit significant plasticity, allowing them to integrate signals from diverse sources. Broadly, three key factors influence macrophage polarization: epigenetic pathways that regulate macrophage development and viability, the tissue microenvironment, and extrinsic factors such as microbial products and cytokines released during inflammation (Murray, 2017).

As mentioned above, macrophages are part of the innate immune system; within this context, they function as antigen-presenting cells and phagocytose pathogens or cellular debris (Li et al., 2023). For example, inflammatory activated macrophages express costimulatory receptors for components of the adaptive immune system, such as T cells, via the co-stimulatory interactions of CD80 and CD86 expressed on macrophages along with their ligands CD28 and CD152 on T cells, necessary for T cell survival and activation (Lenschow et al., 1993). Traditionally, macrophages have been characterized using a simple “M1,” “M2,” and “M0” classification system, with M1 being pro-inflammatory, M2 representing anti-inflammatory, and M0 denoting the steady state (Yunna et al., 2020). While this classification is useful, it was developed in the pre-genomic era when only a few markers were available to gauge macrophage responses, and it does not necessarily represent true *in vivo* conditions (Martinez & Gordon, 2014). In fact, *in vivo*, we observe a much broader spectrum of macrophage polarization, with varying degrees of pro- and anti-inflammatory markers, influenced by multiple cellular and environmental factors (Xue et al., 2014). This is especially pronounced in tumor-associated macrophages (TAMs), which are often unfit for a binary M1/M2 classification (Murray, 2017, Saha et al., 2024). TAMs represent a significant portion of pro-inflammatory infiltrates in neoplastic tissues. They are monocyte-derived and are recruited via monocyte chemotactic

protein chemokines (Singh et al., 2021). TAMs fulfill two seemingly opposing roles in the TME. On the one hand, they can directly kill and phagocytose neoplastic cells following activation by pro inflammatory signals from interferons or interleukins, exhibiting clear anti tumorigenic properties (DeNardo & Ruffell, 2019;). On the other hand, TAMs produce pro-tumorigenic cytokines, MMPs, and growth factors that stimulate angiogenesis and lymphangiogenesis, all of which are linked to neoplastic progression (Qian & Pollard, 2010; Galdiero et al., 2013; Saha et al., 2024). Additionally, TAMs secrete IL-10, which hampers cytotoxic T cell responses and therefore impairs tumor clearance (DeNardo & Ruffell, 2019). In melanoma models, TAMs have been shown to produce TNF-α and IL-1α. In responses to these stimuli, melanocytes produce IL-4 and VEGF-A, which act as potent growth factors that regulate vascular angiogenesis and create a more permeable vasculature, thereby linking macrophage infiltration with tumor progression (Habib et al., 2024).

The role of macrophages in tumor progression is more complex than previously understood, as macrophage heterogeneity varies between different tumors and tumor locations (Bied et al., 2023). Moreover, macrophages appear to play distinct roles at different stages of tumor progression. During tumor initiation, pro-inflammatory M1-like TAMs can foster chronic inflammation, creating a mutagenic TME that drives tumor progression, while in later malignant stages, immunosuppressive and growth-promoting signals predominate (Salmaninejad et al., 2019). Therefore, generating a comprehensive understanding of the diverse functions that macrophages perform in the TME is crucial for developing effective anticancer therapies.

1.5 Oxysterols and 27 Hydroxycholesterol

Oxysterols are oxidized derivatives of cholesterol or its precursors, produced either via enzymatic or non-enzymatic processes (Van Reyk et al., 2006). They serve as bioactive molecules and participate in a wide array of pathways and functions, depending on the developmental stage of the organism as well as the specific organ and/or cell type. This includes, but is not limited to, the biologically active form of vitamin D_3, 1α,25 dihydroxy vitamin D_3, which is essential for calcium absorption and proper bone development (Vo et al., 2023). Cerebrosterol, also known as 24S hydroxycholesterol (24(S)-HC), functions as the main cholesterol metabolite in the brain (Schroepfer, 2000). 25 hydroxycholesterol (25-HC) is produced in macrophages in response to bacterial and viral infections and serves important immunological functions (Baumman et al., 2009). Meanwhile, 7α hydroxycholesterol and 27 hydroxycholesterol (27-HC) represent the first members of the neutral and acid pathways of

bile acid synthesis, respectively (Frédéric et al., 2017). Additionally, oxysterols bearing hydroxyl modifications on the sterol side chain of cholesterol, such as 22 (R) hydroxycholesterol, 24(S)-HC, 25-HC, and 27-HC, all, albeit to varying degrees, act as agonists of the liver X receptor (LXR) and thereby contribute to cellular cholesterol homeostasis (Griffiths & Wang, 2019). Although oxysterols participate in numerous biological processes, this work will primarily focus on 27-HC.

1.4.1. Production of 27-HC

There are two key enzymes that maintain the local concentration of 27-HC in tissues; namely Cytochrome P450 family 27 subfamily A member 1 (CYP27A1), the enzyme that catalyzes the conversion of cholesterol into 27-HC (Figure 1), and Cytochrome P450 family 7 subfamily B member 1 (CYP7B1), the enzyme that metabolizes 27-HC into 7-alpha,27-hydroxycholesterol (Kim et al., 2022). 27-HC shares nearly the same molecular structure as its substrate cholesterol, except for the key addition of a hydroxyl-group at the 27/26 carbon atom, which introduces an extra chiral center and forms a reactive group (Figure 1). Side chain oxysterols are predominantly produced enzymatically, in contrast to oxidation events mediated by environmental oxygen. Furthermore, due to the reactive nature of oxysterols, obtaining precise concentration estimates is challenging; however, 27-HC is consistently the most abundant oxysterol found in humans (Van Reyk et al., 2006).

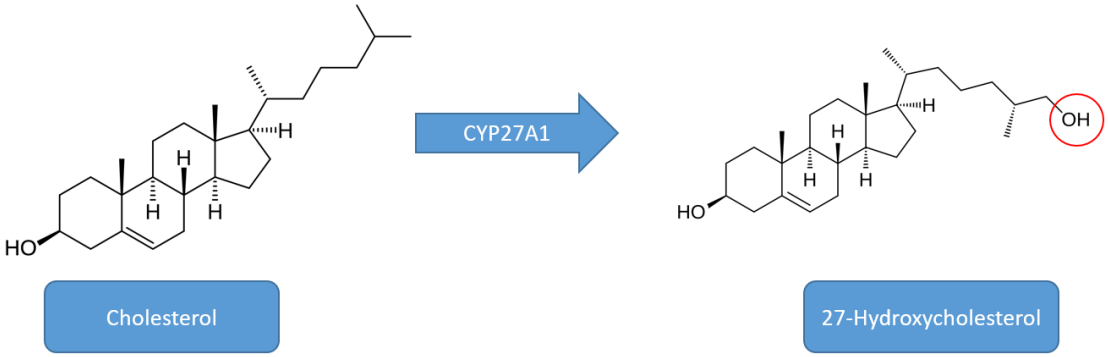

Figure 1. Enzymatic reaction depicting cholesterol transition to 27-Hydroxycholesterol catalyzed by CYP27A1
Red circle depicts hydroxyl-group addition in the sterol side chain of 27-HC

1.4.2. 27-HC and Cancer

The role of 27-HC in cancer physiology is currently only partly understood and appears to vary significantly depending on the type of cancer. It has been proposed as a link between obesity, hypercholesterolemia, and the increased incidence of cancer in individuals with these comorbidities (Asghari & Umetani, 2020). Despite decades of research, the mechanism linking hypercholesterolemia and carcinogenesis remains incomplete and is paradoxically marked by conflicting results. Several studies have reported that low serum cholesterol or the use of cholesterol lowering drugs (statins) is associated with a lower risk of cancer and even protective effects (Llaverias et al., 2011; Pelton et al., 2012), whereas others have found no significant difference or even adverse, carcinogenic outcomes (Bjerre et al., 2001; Ravnskov et al., 2012).

To focus more directly on 27-HC, which is recognized as the first endogenous selective estrogen receptor modulator (SERM), its role in promoting ER positive breast cancer has been widely studied and accepted (Kim et al., 2022; Abdalkareem et al., 2022). In contrast, studies analyzing prostate cancer in humans have found conflicting results, with the majority reporting favorable outcomes for 27-HC (Biasi et al., 2022). While research on prostate and breast cancer, two generally hormone sensitive malignancies have advanced considerably, the effect of 27-HC on other cancers in human settings remains sparse. Nonetheless, from the few human studies available, a general tumor promoting trend can be observed in colon cancer (Rossin et al., 2019), melanoma (Tian et al., 2018), and thyroid adenoma (Revilla et al., 2019). It should be noted, however, that in some of these studies the overall number of biological replicates was low and/or significantly increased 27-HC concentrations were observed only in advanced stages of cancer (Biasi et al., 2022). Additionally, no analysis was performed regarding the specific source of 27-HC in the TME in these studies.

1.4.3. 27-HC as a Regulator of Cellular Cholesterol Homeostasis

All mammalian cell membranes are primarily composed of phospholipids, which exhibit an amphiphilic character by possessing long hydrophobic side chains and polar, hydrophilic regions. This inherent property allows phospholipids to self-assemble into stable lipid bilayer membranes (Brett et al., 2011). The composition of the lipid bilayer has major impacts on cellular functions, either by altering the fluidity of the membrane itself or by allowing phospholipids to serve as signaling molecules (Brett et al., 2011). As an example, it has been demonstrated that membrane fluidity and cholesterol composition regulate adenylate cyclase activity, an enzyme that catalyzes the critical signaling molecule cAMP from ATP (Houslay et

al., 1987). Meanwhile, phosphatidylinositol (4,5)-bisphosphate (PIP_2) and phosphatidylinositol (3,4,5)-trisphosphate (PIP_3) function as messengers in membrane-cytoskeletal interactions (Czech, 2000). There are several abundant and minor phospholipids constituting mammalian cell membranes, but cholesterol remains the sole major sterol present (Goodman et al., 2008). Due to its molecular structure, cholesterol possess a sterol side chain attached to four rings fused in a trans configuration, providing a hydrophobic, rigid structure, while its hydroxyl group confers an amphiphilic character, allowing it to be readily incorporated into cell membranes (Figure 1). Therefore, cellular cholesterol homeostasis is of vital importance for proper cellular function and viability, and cells expend significant resources regulating their cholesterol levels, through processes such as de novo synthesis, cellular transfer, intracellular storage, efflux, and metabolism of cholesterol (Brett et al., 2011).

Side chain oxysterols, such as 27-HC, impact cellular cholesterol homeostasis via two distinct signaling pathways associated with the LXR and SREBPs. LXRs are sterol-activated transcription factors mainly triggered by oxysterols, with the most abundant being 27-HC. Two isoforms, LXRα (*Nr1h3*) and LXRβ (*Nr1h2*), have been identified (Hong & Tontonoz, 2014). While LXRα is dominantly expressed in metabolically active tissues (e.g., hepatocytes, macrophages, adipose tissue, and the intestine), LXRβ is ubiquitously expressed in all cell types (Hong & Tontonoz, 2014). LXR transcription factors naturally form heterodimeric complexes with the retinoid X receptor (RXR) and are maintained in a basal co-repressor state on the promoter regions of target genes (Svensson et al., 2003). Only after ligand binding, 9-cis retinoic acid to RXR and/or oxysterols to LXR (Figure 2), are co-repressors exchanged for co-activators. Following the recruitment of nuclear receptor co-activator 1 (NCOA1) and activating signal co-integrator 2 (ASC2), a broad array of genes involved in regulating cellular lipid homeostasis is transcribed (Hong & Tontonoz, 2014). For example, under the regulatory control of LXR lies the ATP-binding cassette transporter ABCA1 (Figure 2), a transmembrane transporter responsible for the efflux of cholesterol and phospholipids (Xu et al., 2020), as well as the E3 ubiquitin ligase known as the inducible degrader of LDL receptor (IDOL), which targets the low-density lipoprotein receptor (LDLR) for lysosomal degradation (Zelcer et al., 2009). Cellular cholesterol homeostasis is further regulated by SREBPs.

In brief, an increase in cholesterol concentration in the endoplasmic reticulum (ER) membrane induces a conformational change in the cholesterol sensing protein, SREBP cleavage activating protein (SCAP), which subsequently binds the ER membrane anchor protein Insig-1. This complex retains SREBP in the ER under high cholesterol conditions, whereas under low

cholesterol levels, Insig 1 dissociates from SCAP, releasing the SCAP/SREBP complex. This complex is then transported to the Golgi apparatus, where SREBP is proteolytically activated by specific proteases. The activated N terminal domain of SREBP is subsequently transported into the nucleus, where it functions as a transcription factor for genes involved in cholesterol synthesis and uptake (Figure 2) (Cheng et al., 2018; Xu et al., 2020). This regulatory mechanism is often dysregulated during cancerous growth, largely due to abnormal signaling via AKT or mTORC1, which leads to increased expression of SREBP2 and subsequent cholesterol enrichment, thereby enhancing cancer progression (Eid et al., 2017).

In summary, cellular cholesterol homeostasis is a tightly regulated process involving multiple mechanisms such as cholesterol influx/efflux, de novo synthesis, metabolism, esterification, and conversion. Moreover, these processes are controlled by both cell intrinsic factors and environmental influences, resulting in numerous potential regulatory points that can be disrupted in cancer. While SREBPs drive the transcription of genes for cholesterol uptake and biosynthesis to increase cholesterol levels, LXR stimulates the transcription of genes involved in cholesterol efflux and the suppression of de novo synthesis, leading to a reduction in cellular cholesterol concentrations (Kopecka et al., 2020). Both signaling pathways are interconnected through the cellular cholesterol sensing mechanism, which opens the possibility that tumor induced dysregulation of oxysterols, specifically 27-HC, could have cascading effects on cellular lipid regulation.

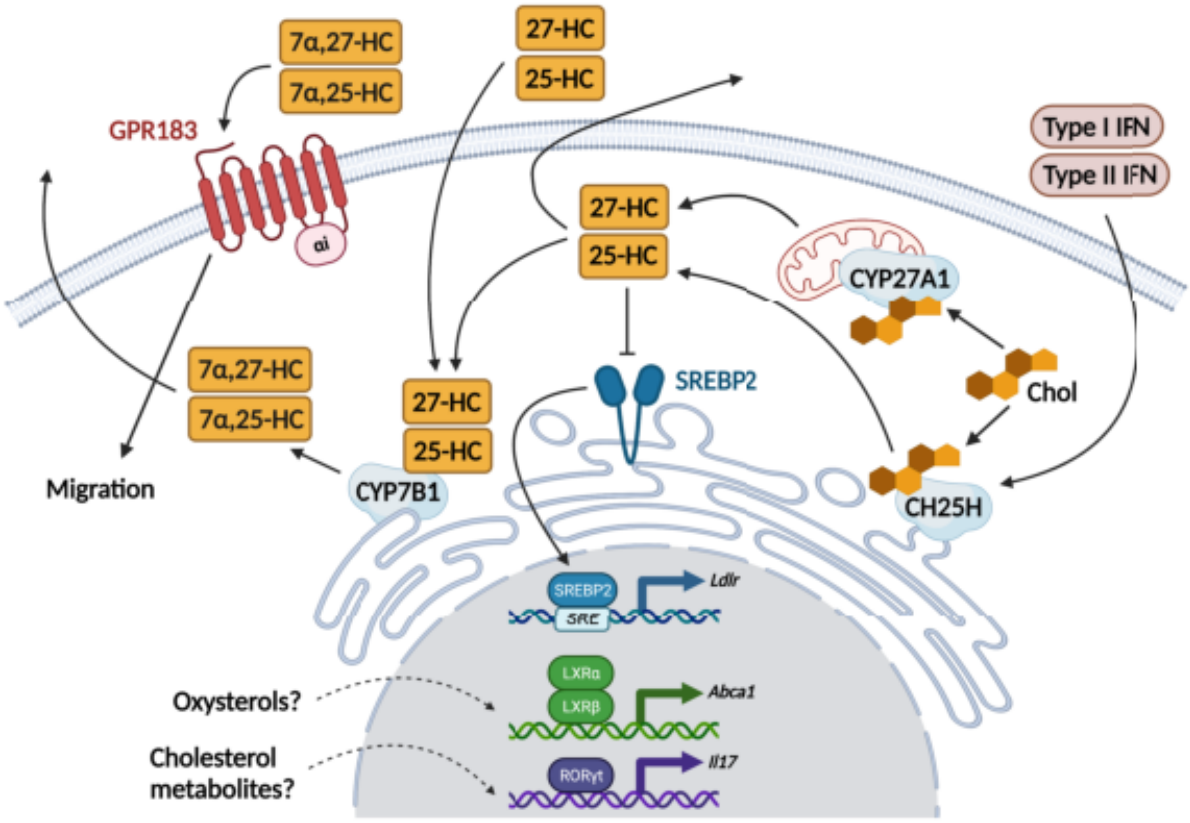

Figure 2. Oxysterol production and sensing.

Note. Reprinted from Dietary cholesterol metabolite regulation of tissue immune cell development and function by M. Frascoli, A. Reboldi, and J. Kang (2022), Journal of Immunology, 209(4), 645–653. Copyright 2022 by the American Association of Immunologists.

Cholesterol (Chol) derived from the diet or produced intracellularly can be metabolized to generate immune-modulating oxysterols. First, the ER-resident enzyme CH25H adds a hydroxyl group at position 25 of cholesterol to synthetize 25-HC. Then in the ER, the cytochrome P450 7B1 (CYP7B1) mediates the hydroxylation at the 7α position of 25-HC to generate 7α,25-HC. GPR183, a GPCR known to mediate migration of several immune cells in tissues, is the receptor for 7α,25-HC. CYP7B1 also produces a second, less potent GPR183 ligand, the oxysterol 7α,27-HC converting 27-HC generated from cholesterol by the mitochondrial enzyme sterol 26-hydroxylase (CYP27A1). Type I and II IFNs induced by viruses and bacteria drive the expression of CH25H. 25-HC restrains the activation of SREBP2 directly in the ER and prevents SREBP2 translocation to the Golgi (not depicted), leading to eventual deficits in the transcription of genes involved in cholesterol metabolism. *In vitro* experiments have suggested that oxysterols can bind to the nuclear receptors LXR (α and β) and retinoic acid receptor–related orphan receptor γ, T isoform (RORγt). Created with BioRender.com

Figure from Franscoli et al., 2022 J Immunol. 2022;209(4):645-653. doi:10.4049/jimmunol.2200273

1.4.4. 27-HC Immunoregulatory Properties

So far, the effect of oxysterols (including 27-HC) as immunoregulatory molecules is only partially understood. The TME is enriched with myeloid cells and lymphocytes, both of which

undergo metabolic reprogramming Specifically, proliferating tumor infiltrating lymphocytes (TIL), such as cytotoxic T cells, upregulate both cholesterol biosynthesis and uptake to support their clonal expansion (Kidani et al., 2013). Meanwhile, the often non proliferative myeloid cells reduce their endogenous cholesterol synthesis while increasing their dependence on cholesterol uptake and scavenging from the TME (York et al., 2015). TIL cholesterol acquisition is correlated with their proliferation rate, and rapid clonal expansion of TIL is critical for effective anti-tumor responses. In fact, cholesterol deficient $CD8^+$ T cells in the TME exhibit an exhaustion associated phenotype, underscoring the importance of cholesterol regulation for robust immune clearance (Yan et al., 2023). Further, Yan et al. (2023) demonstrated that CAR T cells in xenograft models acquire a cholesterol deficient phenotype, with reduced SREBP2 and upregulated LXR levels compared to their *in vitro* counterparts. They also linked the observed phenotype to increased oxysterol concentrations, specifically 27-HC, suggesting that 27-HC may contribute to T cell exhaustion by perturbing the balance of SREBP2/LXR signaling.

Additionally, oxysterols play an important role in mediating the migration of various immune cells. The G-protein coupled receptor (GPCR) GPR183 serves as a receptor for the oxysterol ligands 7α,25-HC and, to a lesser extent, 7α,27-HC, both of which are synthesized from cholesterol via the 25-HC and 27-HC intermediate steps (Figure 2). Signaling through GPR183 is necessary for the proper migration of adaptive and innate immune cells in lymph nodes and the spleen (Franscoli et al., 2022).

1.6 CYP27A1 and Its Role in Cancer

The pathway by which cholesterol is converted into oxysterols, and especially 27-HC, through various cytochrome P450 oxidases is proposed to be the frequently observed link between hypercholesterolemia and cancer progression (Asghari & Umetani, 2020). Within this context, the involvement of CYP27A1 has been investigated *in vitro*, *in vivo*, and in clinical settings (Abdalkareem Jasim et al., 2022). A particularly interesting example comes from Nelson et al. (2013), who demonstrated that in multiple murine models of breast cancer, including the ER positive model MMTV PyMT and an MCF7 human xenograft model, elevated 27-HC concentrations increased tumor size. Furthermore, they showed that genetic deletion of *Cyp27a1* (*Cyp27a1*$^{-/-}$) in MMTV PyMT mice delayed and slowed tumor growth. This effect persisted in *Cyp27a1*$^{-/-}$ mice even when they were fed a high cholesterol diet but could be reversed by daily injections of 27-HC, indicating that 27-HC, rather than cholesterol, is pathological in breast cancer (Nelson et al., 2013).

On the clinical side, Kimbung and colleagues (2020), in two large Swedish population-based breast cancer cohorts, found that *Cyp27a1* expression is associated with an increased risk of ER-positive breast cancer. High expression of *Cyp27a1* in tumors correlated with an overall higher histological grade (in both cohorts) and larger tumor sizes (in one cohort). Worryingly, in younger premenopausal patients, high *Cyp27a1* expression was also linked to a higher recurrence risk within the first five years (Kimbung et al., 2020).

Both studies were performed on breast cancer cohorts or models, where a strong link between 27-HC and its SERM properties has been established in promoting and worsening outcomes (Abdalkareem Jasim et al., 2022). Studies on other malignancies have also been conducted, with similar trends observed in prostate, colon, brain, and lung cancers (Abdalkareem Jasim et al., 2022). These findings underscore the importance of the 27-HC–metabolizing enzymes CYP27A1 and CYP7B1 in maintaining local 27-HC levels and impacting cancer progression.

Interestingly, expression patterns of *Cyp27a1* and *Cyp7b1* show that, at least at low-level expression, these enzymes are almost ubiquitous in the human body, with few exceptions (Asghari & Umetani, 2020). Yet, major reported sources of CYP27A1 activity in the TME are macrophages and the cancer cells themselves (Nelson et al., 2013). Analysis of public single-cell RNA sequencing data from immunotherapy-resistant melanoma (Jerby-Arnon et al., 2018) (Figure 3A) and renal cell cancer (Bi et al., 2021) (Figure 3B) shows that macrophages and TAMs are major sources of *Cyp27a1*-expressing cells in the TME. This observation leads to the hypothesis that macrophage-derived CYP27A1 activity is a major contributor to 27-HC levels in the TME and therefore further exacerbates cancer progression. Much of the research conducted so far has used whole-body *Cyp27a1* knockout models, partly because of their well-established use in bile acid and cholesterol research (Rosen et al., 1998; Nelson et al., 2013; Bhattacharya et al., 2023). While this model is widely used, it cannot distinguish the cellular source of CYP27A1 in the TME. To further clarify the role of 27-HC and CYP27A1 in the TME, a macrophage-specific knockout model is necessary and has been designed.

A ***Cyp27a1* expression in non-malignant cells from human melanoma carcinoma samples**

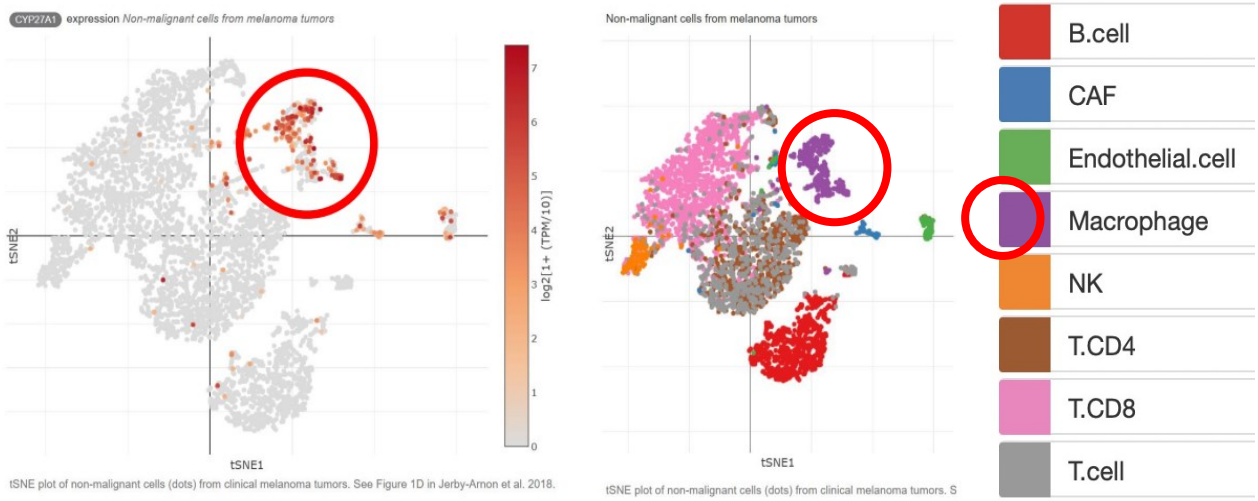

B ***Cyp27a1* expression from human renal cell carcinoma samples**

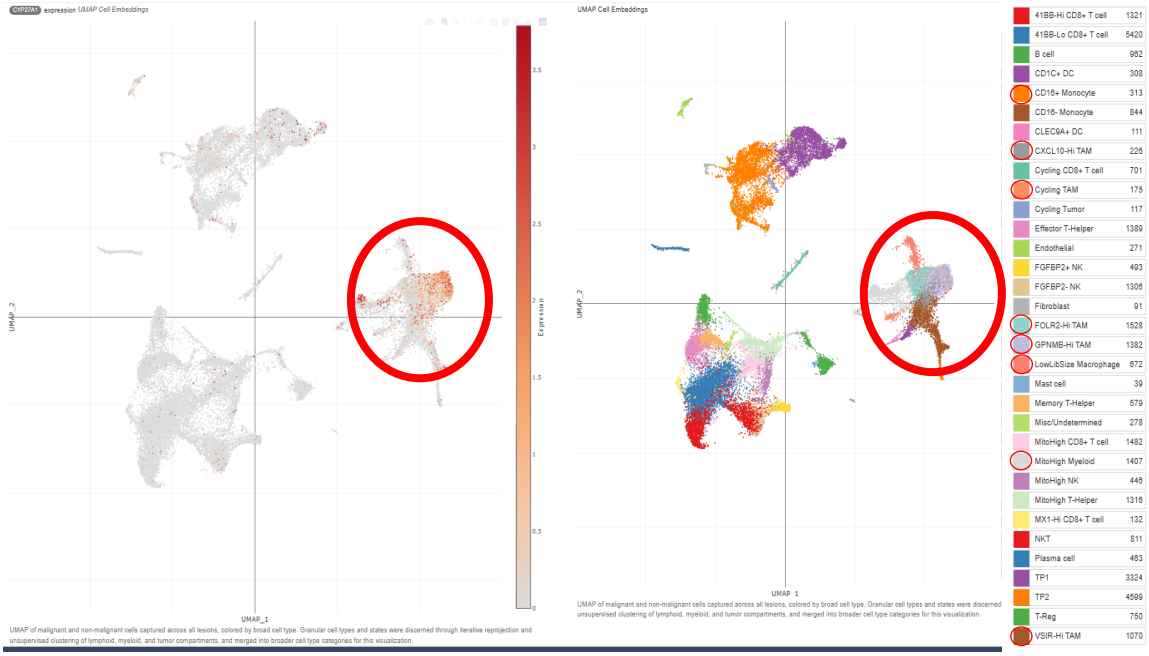

Figure 3. Public single cell RNA data from Jerby-Arnon and colleagues (2018) and Bi and colleagues (2021) shows macrophages and macrophages associated cell populations to be a major source of *Cyp27a1* expression amongst non-malignant cell populations.
(A) *Cyp27a1* expression in non-malignant cells from human melanoma carcinoma samples based on scRNA-seq data from Jerby-Arnon et al., 2018. Left, depicted logarithmic expression heat map of *Cyp27a1*. Right, corresponding cell types as indicated in the legend with macrophages being circled red. Legend top to bottom: B-cells, carcinoma associated fibroblast, endothelia cells, macrophages, natural killer cells, $CD4^+$ T cells, $CD8^+$ T cells and T cells. (B) *Cyp27a1* expression from human renal cell carcinoma samples based on scRNA-seq data from Bi et al., 2021. Left, depicted fold change expression heat map of *Cyp27a1*. Right, corresponding cell types as indicated in the legend. Legend top to bottom with *Cyp27a1* high expressing cell types marked in red, 41BB-Hi $CD8^+$ T cells, 41BB-Low $CD8^+$ T cells, B cells,

CD1C$^+$ dendritic cells, CD16$^+$ monocytes, CD16$^-$ monocytes, CLeC9A$^+$ DC, CXCL10-Hi TAM, cycling CD8$^+$ T cells, cycling TAM, cycling tumor cells, effector T-helper, endothelial cells, FGFBP2$^+$ natural killer cells, FGFBP2$^-$ natural killer cells, fibroblasts, FOLR2-Hi TAM, GPNMB-Hi TAM, LowLibSize macrophages, mast cells, memory T-helper cells, undetermined, Mito High CD8$^+$ T cells, Mito High myeloid cells, cells Mito High natural killer cells, Mito High T-helper cells, MX1-Hi CD8$^+$ T cells, natural killer T cells, Plasma cells, TP1, TP2, T-Reg, VSIR-Hi TAM.

1.7 Research Goal and Outlooks

Taking everything into consideration, we propose that macrophage derived CYP27A1 activity in solid tumor settings is an intriguing target for modulating tumor progression toward more favorable outcomes. This approach could potentially facilitate faster translation into clinical practice, given that FDA approved antihypertensive drugs, such as felodipine and nilvadipine, which inhibit CYP27A1 function through their 1,4 dihydropyridine scaffold, are already available (Lam et al., 2018).

To test this hypothesis, we generated a macrophage-specific knockout model in C57BL/6 mice, in which *Cyp27a1* is flanked by *LoxP* sequences and Cre recombinase is driven by the *Cx3cr1* promoter. The chemokine receptor Cx3CR1 is broadly expressed throughout the mononuclear phagocyte system in mice, including monocytes, macrophages, and certain subsets of T cells, natural killer cells, dendritic cells, and microglia of the central nervous system (Imai et al., 1997). Although a truly macrophage-exclusive expression system does not yet exist, *Cx3cr1*-based approaches have been widely used in macrophage studies (Yona et al., 2013; Sahasrabuddhe & Ghosh, 2022; Jia et al., 2022).

In this thesis, we demonstrate that macrophage-derived CYP27A1 activity in two different solid tumor models (B16 melanoma and MC38 colon adenocarcinoma) contributes to enhanced tumor progression *in vivo*. Furthermore, we characterize the TME of our melanoma model by employing fluorescence-activated cell sorting (FACS) and immunofluorescence (IF) staining, providing evidence of metabolic dysregulation in tumors from our knockout mice. Additionally, through various *in vitro* and *in vivo* experiments, we show that the observed tumor-growth–deficient phenotype is macrophage driven and begin to uncover the underlying mechanism. Finally, we validate our C57BL/6J *Cyp27a1*$^{fl/fl}$ *Cx3cr1*$^{Cre/+}$ (*Cyp27a1*$^{\Delta Cx3cr1\text{-}Cre}$) knockout line and its control counterpart, C57BL/6J *Cyp27a1*$^{fl/fl}$ *Cx3cr1*$^{+/+}$ (*Cyp27a1*$^{fl/fl}$), as suitable models for future macrophage-specific investigations of oxysterols and their roles within the TME.

2. Material and Methods

2.1 Mice Handling and *In Vivo* Studies

C57BL/6J *Cyp27a1*$^{fl/fl}$ *Cx3cr1*$^{Cre/+}$ (*Cyp27a1*$^{\Delta Cx3cr1\text{-}Cre}$) and *Cyp27a1*$^{fl/fl}$ *Cx3cr1*$^{+/+}$ (*Cyp27a1*$^{fl/fl}$) mice were housed at the Centre for Pathobiochemistry and Genetics, Währingerstraße 10, 1060 Vienna. B16 melanoma and MC38 colorectal adenocarcinoma cell lines were subcutaneously injected using 5 * 10^5 cells in phosphate-buffered saline (PBS) mixed 1:1 with Matrigel. The health and tumor growth of mice were periodically monitored and evaluated. Tumors and all organs of interest were harvested after euthanasia by cervical dislocation. Mice were housed under a 12-hour light/dark cycle in a temperature- and humidity-controlled room. Both male and female mice were used randomly. All animal studies were approved by the official Austrian ethics committee for animal experiments.

2.2 Isolation of Bone Marrow–Derived Macrophages (BMDMs)

Bone marrow was isolated from the femur and tibia and differentiated for 6 to 7 days in non-tissue-culture (TC) treated petri dishes (CytoOne). Differentiating macrophages were kept in Roswell Park Memorial Institute (RPMI) 1640 GlutaMAX™ (Gibco) medium supplemented with 100 U/mL penicillin, and 100 µg/mL streptomycin (1× P/S), 10 % fetal bovine serum (FBS) and 30 ng/mL macrophage colony-stimulating factor (M-CSF) (Thermo Fisher). After 3 days, the medium was exchanged, and non-adherent cells were removed. Differentiated macrophages were harvested using PBS-based enzyme-free cell dissociation solution (Merck) and further treated or analyzed as specified.

Alternatively, isolated bone marrow was washed with PBS supplemented with 2% FBS and resuspended in pure FBS. Resuspended cells were transferred to cryotubes containing dimethyl sulfoxide (DMSO) to achieve a final FBS:DMSO ratio of 90:10, and stored overnight (O/N) at –80°C. They were then transferred to liquid nitrogen for long-term storage.

To thaw, cryovials containing bone marrow cells were warmed at 37°C and immediately transferred into 10 mL of prewarmed RPMI medium and washed before being transferred into full macrophage differentiation medium. Cells were then plated on non–TC-treated petri dishes as described above.

2.3 Isolation of Cell Cultures

Murine B16 melanoma cells were maintained in Dulbecco's Modified Eagle Medium (DMEM) supplemented with 10% FBS and 1× P/S, and they were cultured on TC-treated petri dishes. B16 cells were split at 80–100% confluency. All cell cultures were maintained under humid conditions at 37°C and 5% CO_2. The murine MC38 colorectal adenocarcinoma cell line was generously provided by partners from the Dolzing lab in the Institute of Medical Genetics, Medical University of Vienna.

2.4 RNA Isolation, Reverse Transcription, and Real-Time qPCR

$1*10^6$ BMDM were cultivated and either left unstimulated or stimulated with IL-4 (20 ng/mL, Thermo Fisher) or B16 supernatant for 24 hours (Liu et al., 2023). RNA was isolated using the RNeasy kit (QIAGEN) according to the manufacturer's protocol, and its concentration was determined using the Qubit Flex Fluorometer (Invitrogen). 100 ng RNA was reverse transcribed using the GoScript™ Reverse Transcription System kit with random primers (Promega). qRT-PCR was performed on a QuantStudio 3 (Applied Biosystems) using GoTaq® qPCR Master Mix (Promega). Samples were normalized to *β-actin* expression. All primer sequences used are listed in Supplementary Table 4 (Table 4).

2.5 Protein Isolation and Immunoblotting

Cultured BMDMs were washed with ice-cold PBS and scraped into lysis buffer (20 mM HEPES pH 7.9, 0.4 M NaCl, 25% (v/v) glycerol, 1 mM EDTA, 0.5 mM Na_3VO_4, 0.5 mM DTT, 1% Triton X-100) supplemented with protease and phosphatase inhibitors (Roche), 4 µg/mL aprotinin, 4 µg/mL leupeptin, 0.6 µg/mL benzamidine chloride, 20 µg/mL trypsin inhibitor, and 2 mM PMSF (all from Sigma Aldrich). Protein concentrations were determined using the Bradford method (Thermo Fisher) according to the kit's instructions. Equal amounts of protein were loaded on a 12% SDS-PAGE gel and separated via electrophoresis using the Bio-Rad Mini-Trans-Blot Cell System. Proteins were transferred onto nitrocellulose membranes using Bio-Rad Trans-Blot Turbo in semi-dry mode. Membranes were blocked in Intercept Blocking Buffer TBS (LI-COR) for 1 hour on an orbital shaker at 4°C and incubated with primary antibodies overnight. Secondary antibodies were used at a 1:20,000 dilution for 1 hour at room temperature (RT), and membranes were scanned on an Odyssey® CLx scanner at the highest resolution.

2.6 Genotyping

To confirm the genomic background of all mouse-derived samples, small pieces of tail or ear tissue were dissolved in either Direct PCR Tail (VIAGEN) or Direct PCR Ear (VIAGEN) with 1:100 Proteinase K (Thermo Fisher) for 5 hours at 55°C. Enzymes were then inactivated at 85°C for 45 minutes, and samples were stored at –20°C. Confirmation of Cre recombinase and *LoxP* sites in the samples was performed by PCR with the appropriate primers.

2.7 Phagocytosis Assay

B16 melanoma cells were harvested at approximately 80% confluence and stained using the CellTrace™ CFSE kit (Thermo Fisher) following the manufacturer's protocol. Stained cells were kept in DMEM for 30 minutes at 37°C and 5% CO_2. After CFSE labeling, cells were washed thoroughly and incubated with fully differentiated BMDMs for 3 hours in 12-well TC-treated plates under the desired conditions. Cells were then harvested and stained simultaneously for viability (at 1:2000 dilution) and F4/80 (at 1:1000 dilution) at RT for 15 minutes. Stained cells were either fixed with the Foxp3 Fixation/Permeabilization solution kit (Thermo Fisher) or immediately resuspended in PBS for flow cytometric analysis. All samples were measured on a CytoFLEX S (Beckman Coulter) and analyzed using CytExpert software (Version 2.4.0.28).

2.8 Flow Cytometry

Tumor samples were finely minced with a blade, digested in 0.125 mg/mL Collagenase D at 37°C for 90 minutes, and filtered through a 70 µm strainer. For cytokine analysis, cell suspensions were incubated in RPMI medium supplemented with FCS and 1× P/S, then stimulated with PMA/ionomycin and Brefeldin A (BioLegend) for 4 hours. Stainings were performed in 96-well V-bottom plates (Greiner). For dead-cell exclusion, samples were stained with Fixable Viability Dye eFluor™ 780 (Thermo Fisher), washed, and then incubated with surface FACS antibodies (Table 1) for 15 minutes at RT. If intracellular targets were analyzed, cells were washed again, fixed, and permeabilized using the Foxp3 Transcription Factor Staining Set (Invitrogen) according to the manufacturer's protocol, and then incubated overnight at 4°C with antibodies against intracellular targets. All samples were recorded using the CytoFLEX S (Beckman Coulter) and analyzed with CytExpert (Version 2.4.0.28).

2.9 Immunohistochemistry/Immunofluorescence

Either paraformaldehyde- or O.C.T.-embedded sections were analyzed. Mouse tissue was fixed in 4% buffered paraformaldehyde overnight at 4°C, dehydrated in isopropanol, cleared in Xylenol using the KOS Microwave HistoSTATION (Milestone), and finally infiltrated with paraffin prior to embedding. Alternatively, freshly harvested samples were embedded in O.C.T. compound, frozen on dry ice, and then stored at –80°C. Paraffin embedded tissues were sectioned at 3 µm using a microtome (Micros). O.C.T. tissues were sectioned at 5 µm using CryoStar™ NX50 Cryostat (Epredia).

For analysis, paraffin sections were cleared by incubating at 60°C until the paraffin melted, followed by three washes in Neo-Clear (Thermo Fisher). Sections were rehydrated by sequential incubation in 100% and 96% ethanol, then distilled H_2O. Heat-induced epitope retrieval was performed in IHC Antigen Retrieval Solution (low pH) (Thermo Fisher) by autoclaving. Sections were then blocked in 2.5% donkey serum and incubated overnight at 4°C with the indicated primary antibodies (Table 2). O.C.T.-embedded sections were incubated for 10 minutes at RT, then fixed in Histofix (Carl Roth) for 10 minutes. Afterwards, stained and analyzed equal to paraffin embedded sections.

For immunohistochemistry, sections were biotin-blocked by treatment with streptavidin and biotin (Vector Laboratories) according to the kit's guidelines. Biotinylated secondary antibodies were added for 60 minutes, followed by washing with PBST and incubation with HRP-conjugated streptavidin (Leica) for 30 minutes and AEC-high sensitivity substrate (BioLegend) for 4.5 minutes. FILTERED Meyer's Hematoxylin was used for 1 minute for nuclear counterstaining. Sections were mounted using Aquatex (Microscopy) and imaged on an Olympus BX63 Intelligent Microscope; data were analyzed with QuPath™ 0.5.1.

For immunofluorescence staining, after primary antibody incubation, samples were washed in PBST, then incubated with a fluorescently labeled secondary antibody and 4′,6-diamidino-2-phenylindole (DAPI) (Merck) for 45 minutes at RT. After washing in PBST and PBS, sections were mounted in Fluoromount (Sigma Aldrich). Imaging was performed on an Olympus BX63 Intelligent Microscope, and data analysis was conducted with QuPath™ version 0.5.1.

2.10 SCENITH™

BMDMs were cultivated as described above. Three 96-well plates were prepared: (1) one with $1 * 10^5$ macrophages per well in RPMI 1640 GlutaMAX™ (Gibco); (2) one with pre-pipetted inhibitors 2-deoxy-D-glucose (2-DG, final concentration 100mM), oligomycin (O, final

concentration 1µM), both (DGO), or DMSO as control; and (3) one containing puromycin (final concentration 10 µg/mL). All plates were warmed to 37°C. Cells were rapidly transferred onto the inhibitor plate and incubated for 15 minutes at 37°C. DGO was achieved by incubating cells in 2-DG for 10 minutes and then combining them with oligomycin for 5 minutes. Cells were then transferred onto the puromycin plate and incubated for 30 minutes at 37°C. Puromycin incorporation was halted by adding ice-cold PBS and pelleting the cells (500 × g, 4°C, 5 minutes). Macrophages were then stained with Fixable Viability Dye eFluor™ 780 (Thermo Fisher) and FACS surface antibodies (Table 1) as indicated. The Foxp3 Transcription Factor Staining Buffer Set (Invitrogen) was used to fix the cells according to the manufacturer's instructions. Cells were resuspended in Perm Buffer (Invitrogen) with 1:1000 anti-puromycin antibody (Merck) and incubated overnight at 4°C. The next day, cells were washed twice in Perm Buffer, resuspended in PBS, and analyzed on a CytoFLEX S (Thermo Fisher) using CytExpert software (Version 2.4.0.28).

2.11 Lipid Droplet Determination Assay

O.C.T.-preserved samples were sectioned at 5 µm using the CryoStar™ NX50 Cryostat (Epredia) and stored at –20°C until use. Sections were incubated for 10 minutes at RT, then fixed in Histofix (Carl Roth) for 10 minutes. All wash steps were conducted in PBS. Blocking was done with 2.5% donkey serum in PBS for 30 minutes at RT. Primary antibodies were added at working concentrations (Table 2) and incubated overnight. On the following day, secondary antibodies (Table 3), DAPI (1:100), and BODIPY™ 493/503 (1:500, Thermo Fisher) were added and incubated in the dark for 1 hour at RT. Sections were subsequently washed and mounted using Fluoromount (Sigma Aldrich). Imaging was performed on a SpectraPlex Confocal Microscope (Leica), and data were analyzed using QuPath™ version 0.5.1.

3. Results

3.1 *Cyp27a1* mRNA Expression and CYP27A1 Protein Levels Are Reduced in *Cyp27a1*$^{\Delta Cx3cr1\text{-}Cre}$ Macrophages

To study the effect of CYP27A1 in macrophages within the TME, we crossed *Cyp27a1*$^{fl/fl}$ mice with transgenic mice expressing Cre recombinase under the control of the *Cx3cr1* promoter, yielding the desired knockout model (*Cyp27a1*$^{\Delta Cx3cr1\text{-}Cre}$) and its littermate control (*Cyp27a1*$^{fl/fl}$). Under steady-state conditions, *Cyp27a1*$^{\Delta Cx3cr1\text{-}Cre}$ mice showed no observable phenotype. Knockout efficiency was confirmed in three ways. First, via genotyping small pieces of tail or ear tissue and confirming the presence of Cre recombinase and *LoxP* sites around the gene of interest *Cyp27a1* (Figure 4A). Second, at the protein level, western blotting was performed on protein lysates obtained from BMDMs (Figure 4B). Third, the loss of *Cyp27a1* was validated at the mRNA level by RT-qPCR (Figure 4C). Protein levels and mRNA were significantly reduced in *Cyp27a1*$^{\Delta Cx3cr1\text{-}Cre}$ cells compared to *Cyp27a1*$^{fl/fl}$, approximately aligning with an expected Cre recombinase efficiency of 70–80%. All data in this study were obtained from confirmed knockouts.

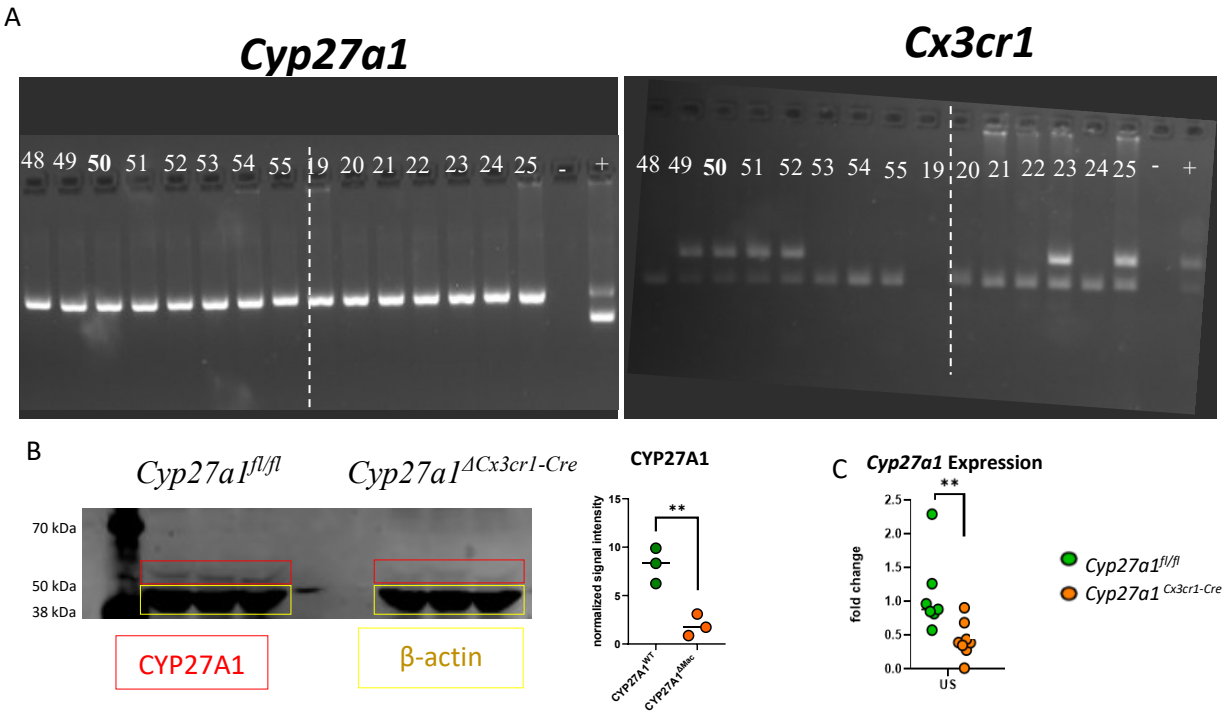

Figure 4. Confirmation of *Cyp27a1*$^{\Delta Cx3cr1\text{-}Cre}$ model used in this study
(A) Agarose gels showing *Cyp27a1* (left) and Cre recombinase downstream of *Cx3cr1* (right).

"+" and "–" denote positive and negative controls, respectively, and numbers indicate mouse ID end digits.
(B) Western blot validation of CYP27A1 protein reduction in BMDMs from *Cyp27a1*$^{fl/fl}$ (left side, n=3) and *Cyp27a1*$^{\Delta Cx3cr1\text{-}Cre}$ (right side, n=3). The red box indicates CYP27A1 (~60 kDa), the yellow box indicates β-actin (~42 kDa). Arrows mark 38, 50, and 70 kDa ladder bands. Quantification to the right is normalized to β-actin.
(C) *Cyp27a1* mRNA levels in *Cyp27a1*$^{fl/fl}$ and *Cyp27a1*$^{\Delta Cx3cr1\text{-}Cre}$ BMDMs, normalized to *β-actin*. $p < 0.01$: **, Data represents the mean.

3.2 *Cyp27a1*$^{\Delta Cx3cr1\text{-}Cre}$ Dampens Growth and Improves Survival of Immunotolerant Melanoma and Immunopermissive Colon Cancer

To examine how Cx3cr1-specific *Cyp27a1*$^{\Delta Cx3cr1\text{-}Cre}$ knockout impacts tumor progression, we inoculated *Cyp27a1*$^{\Delta Cx3cr1\text{-}Cre}$ and *Cyp27a1*$^{fl/fl}$ mice with the immunotolerant murine B16 melanoma cell line (Van Gulijk et al., 2023) and the immune permissive MC38 colon adenocarcinoma cell line (Schrörs et al., 2023). In both models, we observed significantly reduced tumor growth and overall smaller tumor size (Figure 5A, D). Both *Cyp27a1*$^{\Delta Cx3cr1\text{-}Cre}$ and *Cyp27a1*$^{fl/fl}$ showed similar growth and cancer progression up to day 6-7, after which *Cyp27a1*$^{fl/fl}$ *mice* entered exponential growth around day 8 (Figure 5 B, E) while the *Cyp27a1*$^{\Delta Cx3cr1\text{-}Cre}$ mice showed comparable trends after day 15 (Figure 5 B, E). Notably, the B16 tumors displayed a more pronounced growth stagnation compared to MC38. With an overall extended survival rate of 38 % and 25 % for B16 and MC38 respectively when compared to the *Cyp27a1*$^{fl/fl}$ (Figure C, F).

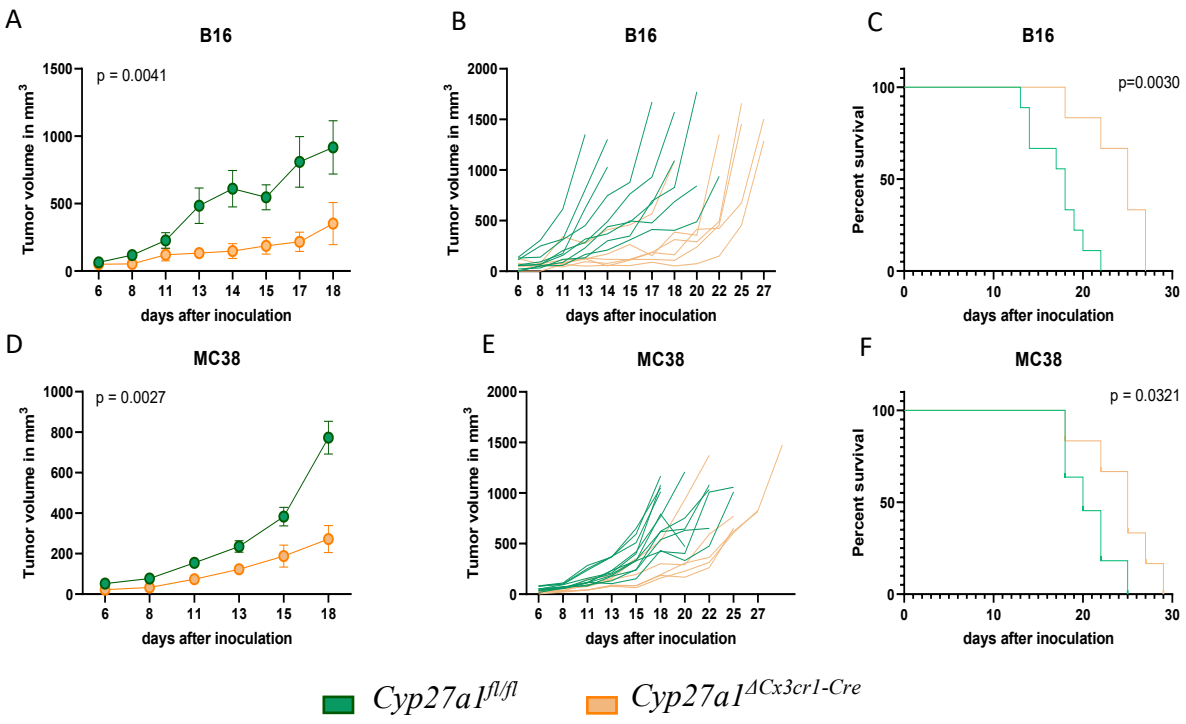

Figure 5. *Cyp27a1*$^{Cx3cr1\text{-}Cre}$ *mice* show dampened tumor growth and extended survival *in vivo*

(A) B16 tumor volume over time in *Cyp27a1*$^{\Delta Cx3cr1\text{-}Cre}$ vs. *Cyp27a1*$^{fl/fl}$ (n=6/9). Statistical significance was determined by mixed-effects model (REML).
(B) Individual B16 tumor growth curves in *Cyp27a1*$^{\Delta Cx3cr1\text{-}Cre}$ vs *Cyp27a1*$^{fl/fl}$
(C) Kaplan–Meier survival for B16-inoculated mice (n=6/9). Statistical significance was determined using Log-rank and Gehan–Breslow–Wilcoxon tests.
(D) MC38 tumor volume over time in *Cyp27a1*$^{\Delta Cx3cr1\text{-}Cre}$ vs. *Cyp27a1*$^{fl/fl}$ (n=6/11). Statistical significance was determined by mixed-effects model (REML).
(E) Individual MC38 tumor growth curves in *Cyp27a1*$^{\Delta Cx3cr1\text{-}Cre}$ vs *Cyp27a1*$^{fl/fl}$.
(F) Kaplan–Meier survival for MC38-inoculated mice (n=6/11). Statistical significance was determined using Log-rank and Gehan–Breslow–Wilcoxon tests

3.3 No Difference in the Lymphoid Compartment of *Cyp27a1*$^{\Delta Cx3cr1\text{-}Cre}$ Mice

Subsequently, we evaluated the immune compartment of the TME from *Cyp27a1*$^{\Delta Cx3cr1\text{-}Cre}$ and *Cyp27a1*$^{fl/fl}$ mice. Because the B16 melanoma model, had a larger reduction in tumor growth compared to the MC38 colon adenocarcinoma model, we reasoned that the effect of the *Cyp27a1*$^{\Delta Cx3cr1\text{-}Cre}$ mice in the B16 model would also be more pronounced. We selected day 12 post-inoculation as a starting point as this was the first time point when statistically significant divergence between *Cyp27a1*$^{\Delta Cx3cr1\text{-}Cre}$ and *Cyp27a1*$^{fl/fl}$ groups was observed (Figure 5A). As proposed by Yan et al. (2023), oxysterols such as 27-HC secreted by the TME can suppress SREBP2 and activate LXR, leading to T cell cholesterol deficiency and dampened cytotoxic

immunity. Contrary to that, our observations revealed no differences in the lymphoid compartment of the TME. To identify the lymphoid compartment, the following gating strategy was applied. First, we gated on CD45$^+$ cells as total immune cells and then identified CD8$^+$ T cells (CD45$^+$, CD3$^+$, CD8$^+$) and CD4$^+$ T cells (CD45$^+$, CD3$^+$, CD4$^+$) (Figure 6).

The overall immune compartment was not impacted in the *Cyp27a1*$^{\Delta Cx3cr1\text{-}Cre}$ TME (Figure 7A). Furthermore, CD8$^+$ T cells populations were similar in both *Cyp27a1*$^{\Delta Cx3cr1\text{-}Cre}$ and *Cyp27a1*$^{fl/fl}$ *cohorts* (Figure 7B). Although a slight trend toward fewer CD4$^+$ T cells in the *Cyp27a1*$^{\Delta Cx3cr1\text{-}Cre}$ TME appeared (Figure 7H), CD4$^+$ and CD8$^+$ populations from both genotypes showed comparable IFN-γ (Figures 7C, I), TNF-α (Figures 7D, J), and PD-1 (Figures 7E, K) levels. Since CD8$^+$ cytotoxic T cells have been identified as key targets for 27-HC-mediated tumor progression (Yan et al., 2023), we further investigated CD103$^+$ (Figure F) and GzmB$^+$ (Figure G) subpopulations. CD103$^+$ cells are known for a longer thymic retention and subsequently increased proliferation (Kutleša S. et al; 2002) while granzyme B (GzmB) is involved in an active tumor clearance (Afonina et al., 2010). Yet despite overall reduced tumor growth no difference between either subpopulation was observed (Figure F, G).

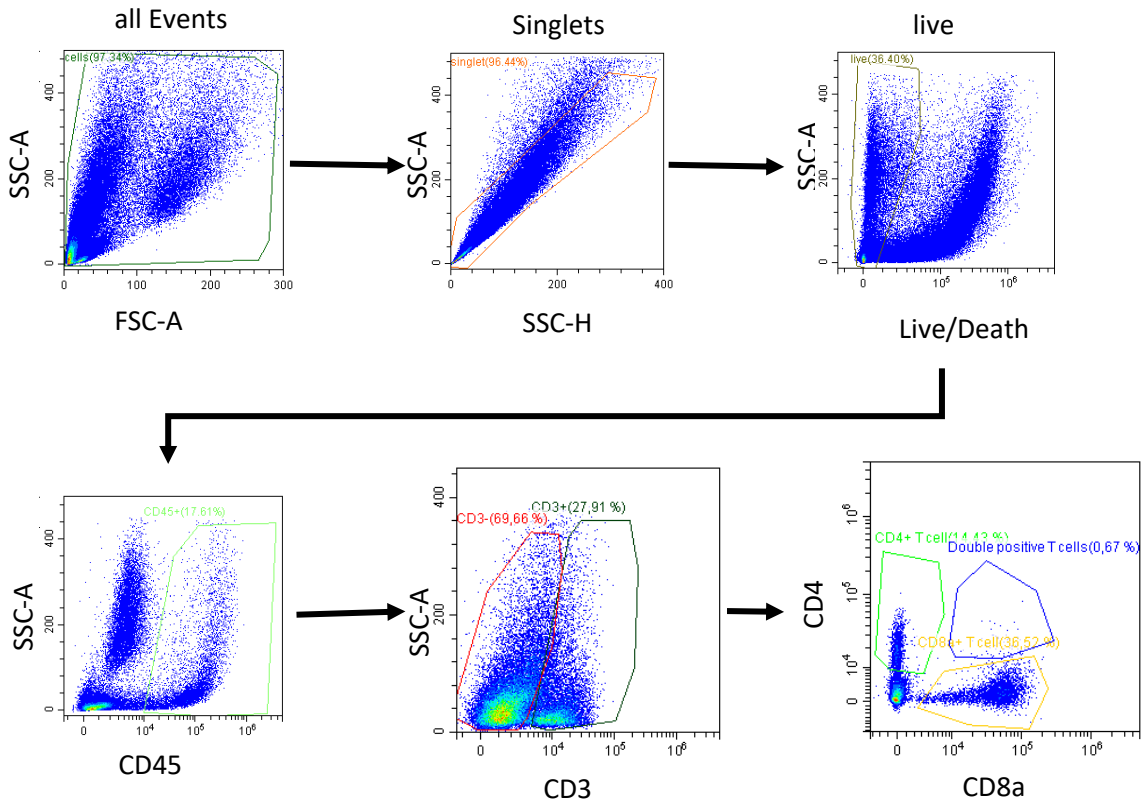

Figure 6. Gating strategy for lymphoid panel
Analysis of *Cyp27a1*$^{fl/fl}$ and *Cyp27a1*$^{\Delta Cx3cr1\text{-}Cre}$ TME cell populations via flow cytometry. Doublets and dead cells were excluded by SSC-H/SSC-A and viability gating. CD8$^+$ T cells were classified as CD45$^+$, CD3$^+$and CD8$^+$. CD4$^+$ T cells were classified as CD45$^+$, CD3$^+$and CD4$^+$.

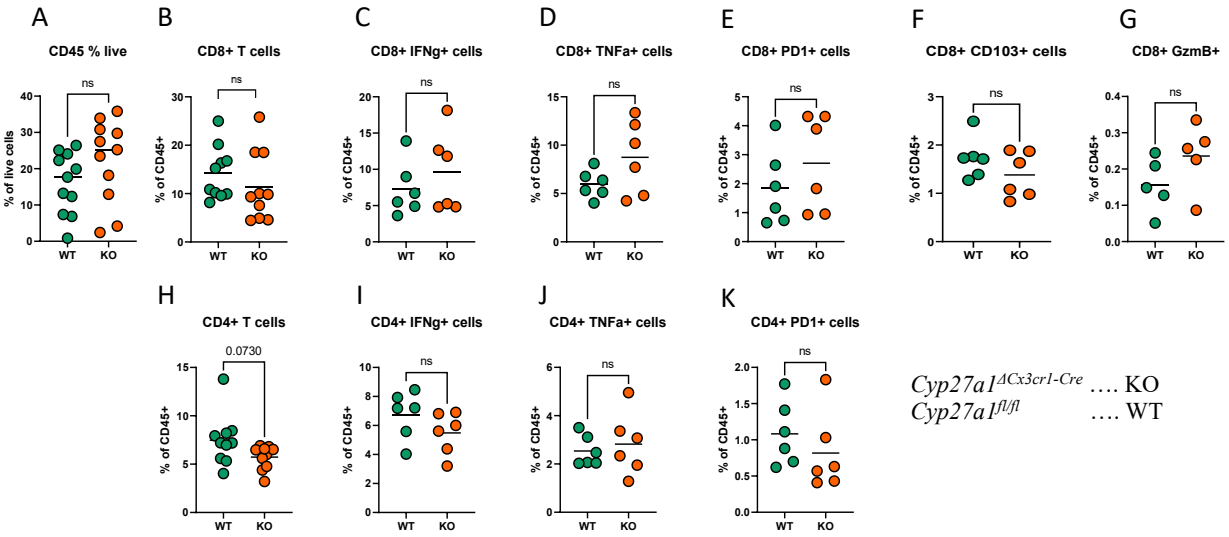

Figure 7. Analysis of lymphoid compartment in the TME of B16 melanoma from *Cyp27a1*$^{fl/fl}$ and *Cyp27a1*$^{\Delta Cx3cr1\text{-}Cre}$ mice

(A) CD45$^+$cells (%) among live cells. *Cyp27a1*$^{fl/fl}$ *vs* *Cyp27a1*$^{\Delta Cx3cr1\text{-}Cre}$ (n =11/11).

(B) CD8$^+$ cells (% of CD45$^+$), *Cyp27a1*$^{fl/fl}$ *vs* *Cyp27a1*$^{\Delta Cx3cr1\text{-}Cre}$ (n =11/11).

(C, D, E, F, G) Further characterization of CD8$^+$ cells for (C) IFN-γ, (D) TNF-α, (E) PD-1, (F) CD103 and (G) GzmB. *Cyp27a1*$^{fl/fl}$ vs *Cyp27a1*$^{\Delta Cx3cr1\text{-}Cre}$ (n = 6/6).

(H) CD4$^+$ cells (% of CD45$^+$), *Cyp27a1*$^{fl/fl}$ *vs* *Cyp27a1*$^{\Delta Cx3cr1\text{-}Cre}$ (n =11/11).

(I, J, K) Further characterization of CD4$^+$ cells for (I) IFN-γ, (J) TNF-α, and (K) PD-1. *Cyp27a1*$^{fl/fl}$ vs *Cyp27a1*$^{\Delta Cx3cr1\text{-}Cre}$ (n = 6/6).

ns = not significant. Data represents the mean.

3.4 Fewer Macrophages in the TME of *Cyp27a1*$^{\Delta Cx3cr1\text{-}Cre}$ Mice

Next, we examined the myeloid compartment in the B16 TME, hypothesizing that *Cx3cr1*-driven *Cyp27a1* knockout would primarily affect macrophages. First, we gated on CD45$^+$ cells as total immune cell. The myeloid compartment compromised macrophages classified as CD11b$^+$, Ly6C$^-$ and F4/80$^+$ cells, monocytes classified as CD11b$^+$, Ly6C$^+$ and SSC-A^{low}/FSC-A^{low} and neutrophils classified as CD11b$^+$, Ly6C$^+$ and SSC-A^{high}/FSC-A^{high} (Figure 8).

Tumors analyzed 12 days post-inoculation in *Cyp27a1*$^{\Delta Cx3cr1\text{-}Cre}$ mice showed a reduced macrophage population present in the TME (Figure 9A). In addition, neutrophils trended downwards (Figure 9B) while monocyte counts were unchanged (Figure 9C). Moreover, *Cyp27a1*$^{\Delta Cx3cr1\text{-}Cre}$ macrophages showed overall reduced expression of tested surface markers (Figure 9D, E, F, G,). *Cyp27a1*$^{\Delta Cx3cr1\text{-}Cre}$ macrophage showed less expression of pro-inflammatory markers CD86 (Figure 9F), a T cell co-stimulator and activator, and CD40

(Figure 9E), which is part of the TNF-receptor superfamily and necessary for T cell-dependent immunoglobulin class switching and germinal center formation (Grewal & Flavell 1998). Additionally, Siglec-1/CD169 was also downregulated (Figure 9D), a lectin which recognizes sialic acid on cell surface glycoproteins and facilitates interaction of macrophages with other cells thereby contributes to antitumor immunity (Kim et al, 2022). Notably, CD206, a "M2" macrophage polarization marker (Scodeller et al., 2017) is similarly downregulated in the *Cyp27a1*$^{\Delta Cx3cr1\text{-}Cre}$ macrophages (Figure 9G). In contrast, MHCII expression remained unchanged (Figure 9H). Altogether, these data indicate *Cyp27a1* expression in macrophages is involved in cellular abundance and cell surface marker expression.

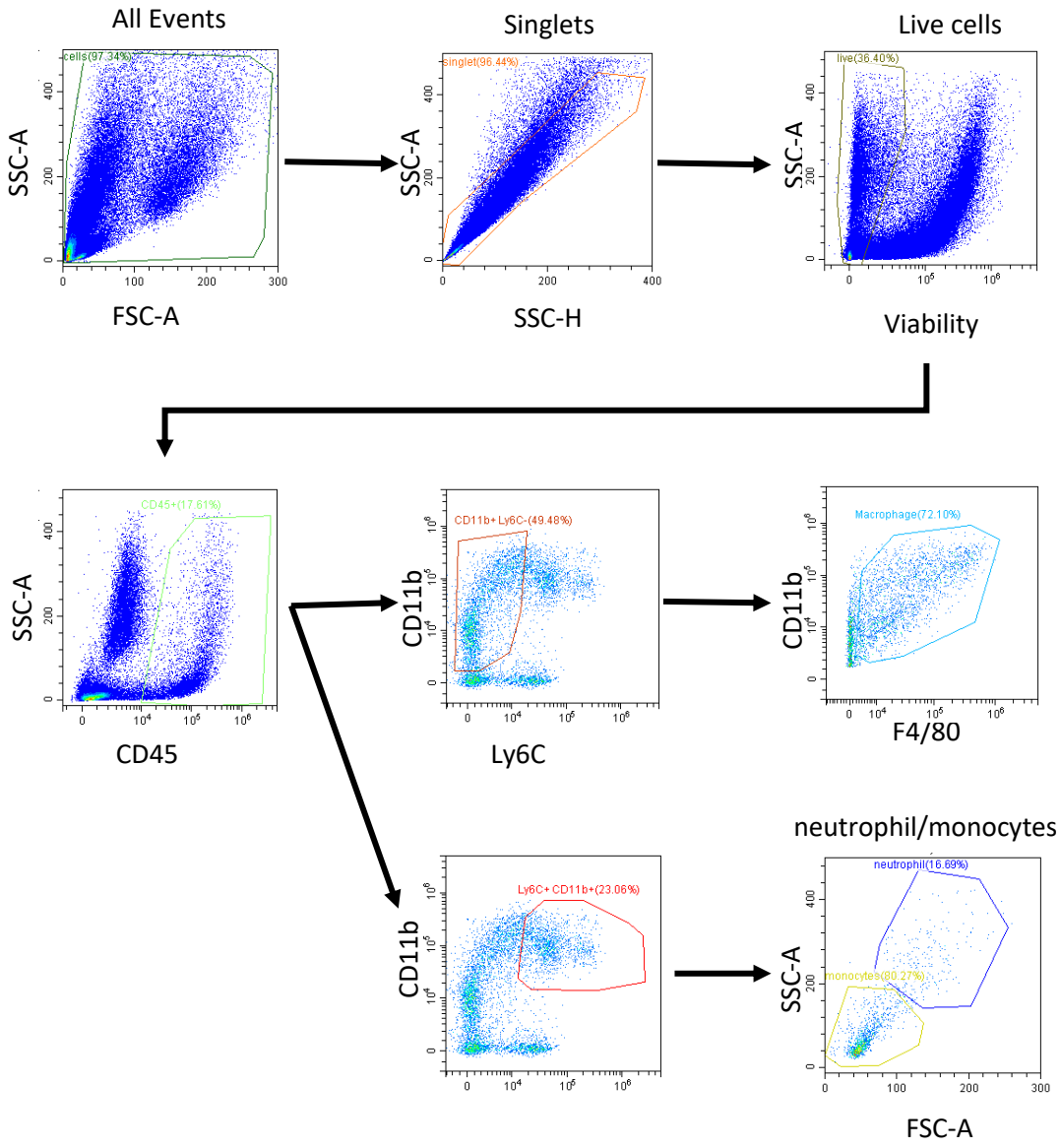

Figure 8. Gating strategy for myeloid panel
Analysis of *Cyp27a1*$^{fl/fl}$ and *Cyp27a1*$^{\Delta Cx3cr1\text{-}Cre}$ TME cell populations via flow cytometry. Doublets and cells dead were excluded by SSC-H/SSC-A and viability gating. Macrophages

were classified as CD45$^+$, CD11b$^+$, Ly6C$^-$ and F4/80$^+$, Neutrophils were classified as CD45$^+$, CD11b$^+$, Ly6C$^+$ large cells (SSC-A^{high}/FSC-A^{high}) Monocytes were classified as CD45$^+$, CD11b$^+$, Ly6C$^+$ small cells (SSC-A^{low}/FSC-A^{low}).

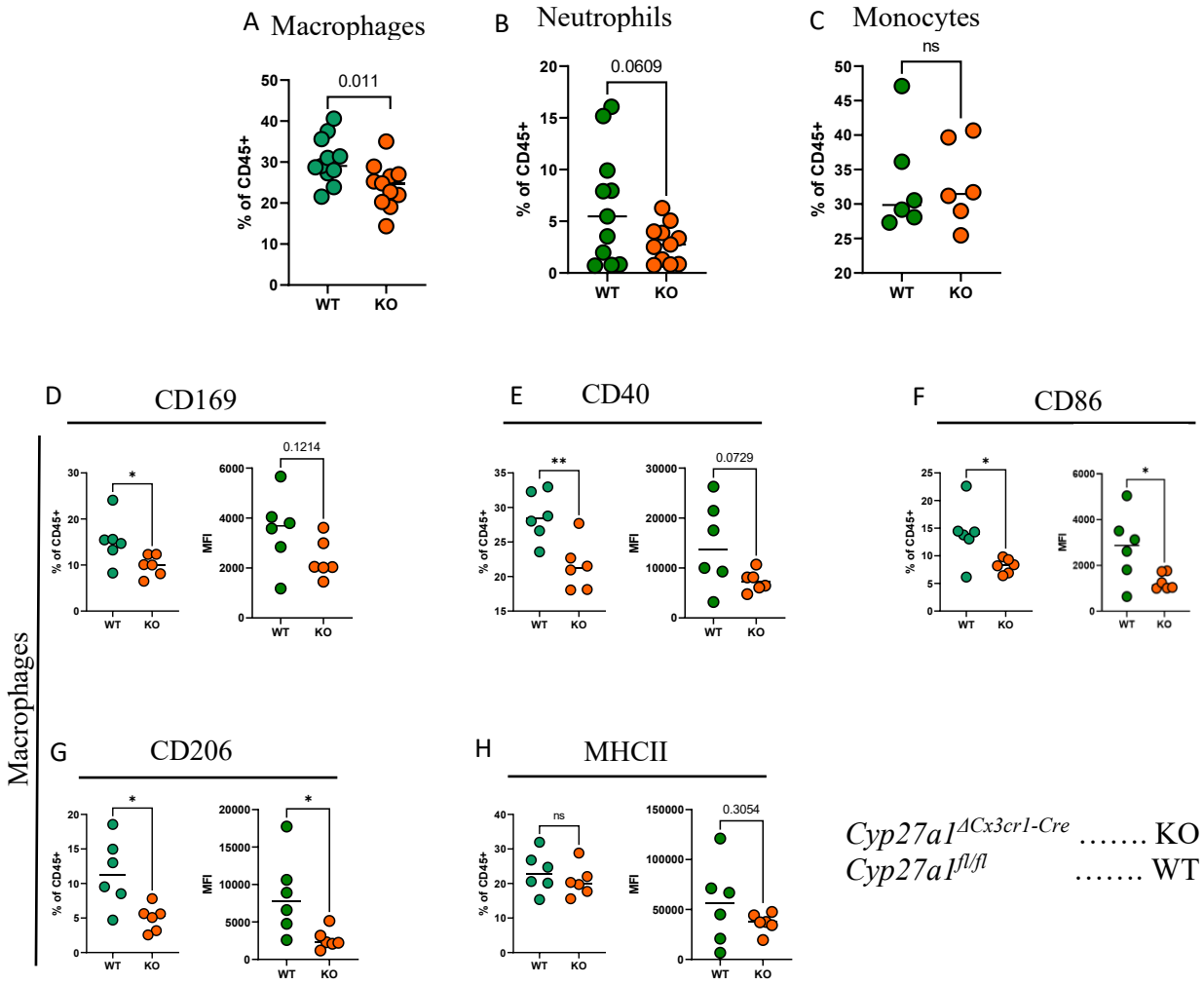

Figure 9. Analysis of macrophage and myeloid compartment in the TME of B16 melanoma from *Cyp27a1*$^{fl/fl}$ and *Cyp27a1*$^{\Delta Cx3cr1\text{-}Cre}$ mice
(A) Macrophages (% of CD45$^+$). *Cyp27a1*$^{fl/fl}$ vs *Cyp27a1*$^{\Delta Cx3cr1\text{-}Cre}$ (n = 11/11).
(B) Neutrophils (% of CD45$^+$). *Cyp27a1*$^{fl/fl}$ vs *Cyp27a1*$^{\Delta Cx3cr1\text{-}Cre}$ (n = 11/11).
(C) Monocytes (% of CD45$^+$). *Cyp27a1*$^{fl/fl}$ vs *Cyp27a1*$^{\Delta Cx3cr1\text{-}Cre}$ (n = 6/6).
(D, E, F, G, H) Further characterization of macrophage for (D) CD169, (E) CD40, (F) CD86, (G) CD206, and (H) MHCII. Data is presented as % of CD45$^+$ (left) and mean fluorescent intensity (MFI, right) *Cyp27a1*$^{fl/fl}$ vs *Cyp27a1*$^{\Delta Cx3cr1\text{-}Cre}$ (n = 6/6).
$p < 0.05$: *, $p < 0.01$: **; ns = not significant. Data represents the mean.

3.5 Increased Lipid Droplet Presence in *Cyp27a1*$^{\Delta Cx3cr1\text{-}Cre}$ Macrophages and Melanocytes?

We aimed to determine whether CYP27A1 deficiency in macrophages influences LD content in the TME, given 27-HC's role as a ligand for LXR which in turn regulates intra and extra

cellular cholesterol shuffling and production. Staining tumor sections with BODIPY™ 493/503 showed an overall increase in LD load in *Cyp27a1*$^{\Delta Cx3cr1\text{-}Cre}$ tumors (Figure 10A) and a slight trend toward larger droplets (Figure 10B). To comprehensively analyze the lipid droplet distribution in the TME we additionally co-stained for CD206, a macrophage marker associated with M2/TAM polarized macrophages (Scodeller et al., 2017), and Sox10, an embryonic cell fate transcription factor which recurred in B16 melanoma cell line (Willis et al., 2015). Which revealed elevated LD content in both macrophages (Figure 10F) and tumor cells (Figure 10E) in the TME of *Cyp27a1*$^{\Delta Cx3cr1\text{-}Cre}$ mice.

Interestingly, the generally smaller tumors in *Cyp27a1*$^{\Delta Cx3cr1\text{-}Cre}$ mice displayed a higher LD burden, a phenotype typically associated with aggressive growth (Jin et al., 2023). Additionally, in *Cyp27a1*$^{fl/fl}$ tumors, approximately 50% of Sox10^{+} cells (Figure 10C) and 40% of CD206^{+} cells (Figure 10E) were LD-negative, versus approximately 25% in the *Cyp27a1*$^{\Delta Cx3cr1\text{-}Cre}$ tumors. Collectively, these data suggest that macrophage-derived 27-HC is crucial for regulating LD content in the TME.

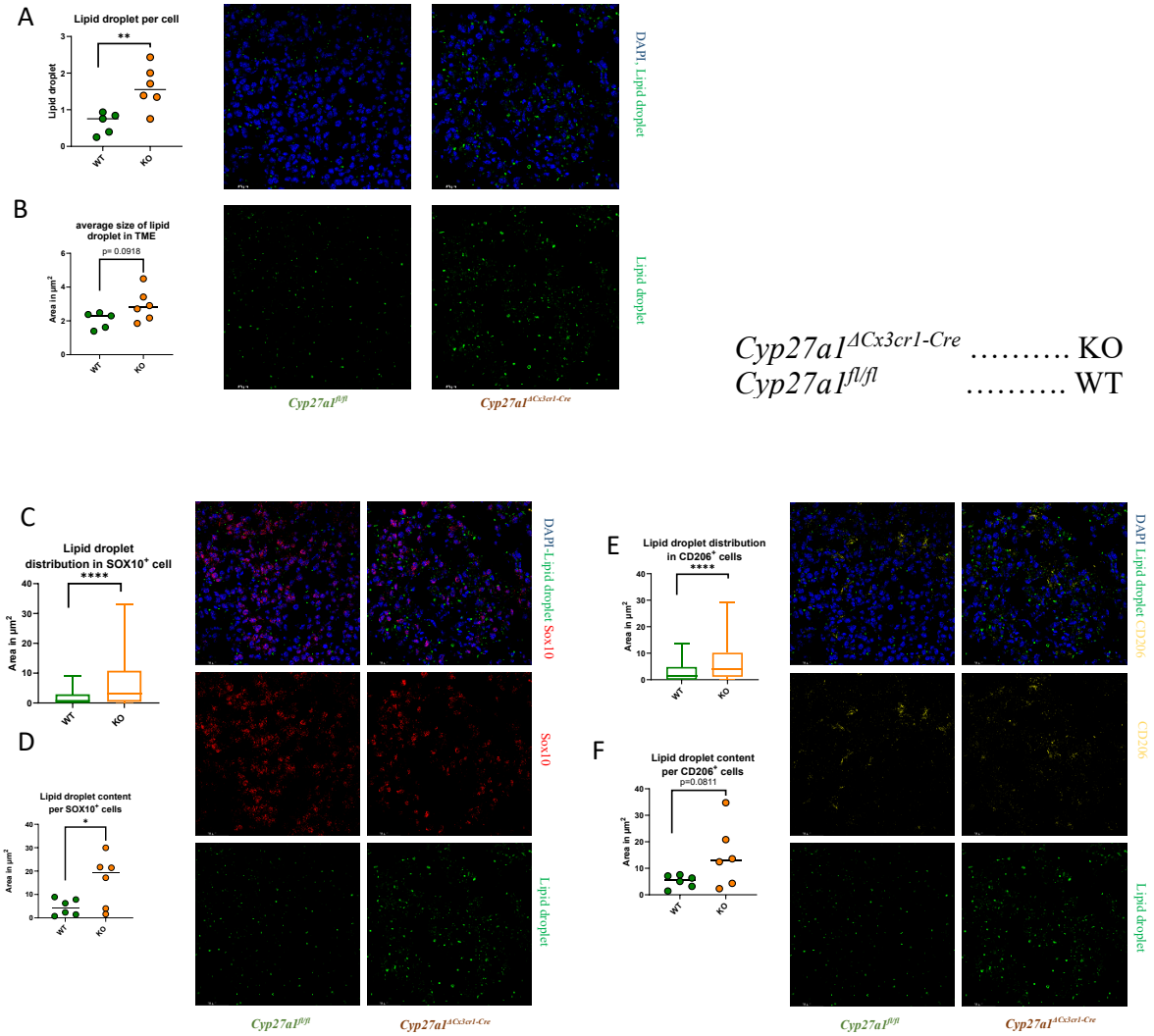

Figure 10. Increased lipid droplet burden in TME of *Cyp27a1*$^{\Delta Cx3cr1\text{-}Cre}$ mice in macrophages and tumor cells
(A, B) Quantification of average LD (A) number and (B) size in µm^2 of BODIPY^{TM}493/503$^+$ cells from *Cyp27a1*$^{fl/fl}$ vs *Cyp27a1*$^{\Delta Cx3cr1\text{-}Cre}$(n=6/6) mice.
(C) Box-Whisker-Plot analysis of the area (in µm^2) of BODIPY^{TM}493/503$^+$ staining for all individual Sox10$^+$ cells.
(D) Average area (in µm^2) of BODIPY^{TM}493/503$^+$ staining of Sox10$^+$ cells per tumor and genotype (n=6/6).
(E) Box-Whisker-Plot analysis of the area (in µm^2) of BODIPYTM 493/503$^+$ staining for all individual CD206$^+$ cells.
(F) Average area (in µm^2) of BODIPYTM 493/503$^+$ staining of CD206$^+$ cells per tumor and genotype (n=6/6).
Per tumor 5-8 random pictures were evaluated. $p < 0.05$: *, $p < 0.01$: ** p **** < 0.0001. Representative images are shown, scale bars, 52 µm. Data represents the mean

3.6 *Cyp27a1*$^{\Delta Cx3cr1\text{-}Cre}$ Tumors show Increased Proliferation Signaling

We next examined tumor sections via immunofluorescence and immunohistochemistry to understand the mechanism behind reduced *in vivo* tumor growth. As our own flowcytometry based analysis of the TME indicated no significant lymphocytes differences (Figure 7A) we looked at other explanations for the observed reduced tumor growth phenotype in our mice model.

We evaluated CD31, an endothelial marker associated with angiogenesis (Lertkiatmongkol et al., 2016). Additionally, cleaved caspase 3 (cCasp3), a key component of the cell-intrinsic apoptotic pathway (Nicholson et al., 1995), and p16^{INK4a}, a marker of cellular senescence enforcing irreversible cell cycle arrest (Safwan-Zaiter et al., 2022), were all assessed in both genotypes. No significant differences were found between *Cyp27a1*$^{\Delta Cx3cr1\text{-}Cre}$ and *Cyp27a1*$^{fl/fl}$ *for* CD31 (Figure 11A) or p16^{INK4a} (Figure 11B). cCasp3 showed a nonsignificant downward trend in the *Cyp27a1*$^{\Delta Cx3cr1\text{-}Cre}$ tumors (Figure 11C).

We then looked at Ki-67, a marker of cell proliferation (Li et al., 2015). Somewhat unexpectedly, the smaller *Cyp27a1*$^{\Delta Cx3cr1\text{-}Cre}$ tumors had a higher percentage of Ki-67$^+$ cells (Figure 11E), while Sox10$^+$ melanoma cells remained comparable (Figure 11F). This suggests that macrophage-specific CYP27A1 deficiency alters proliferation dynamics rather than purely mediating growth arrest.

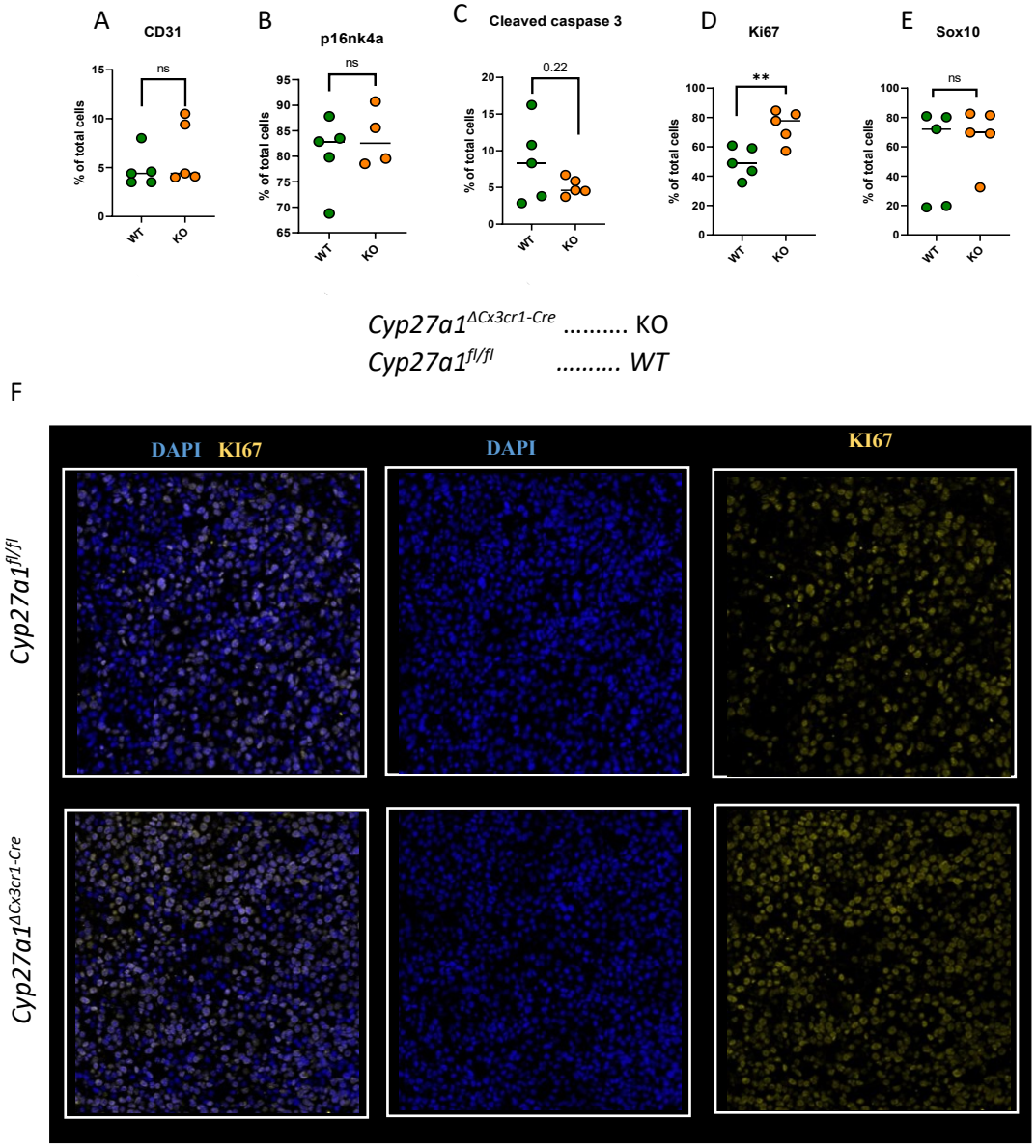

Figure 11. Increased proliferation signaling in TME of *Cyp27a1*$^{\Delta Cx3cr1\text{-}Cre}$ tumors
(A) CD31^{+} cells, (IF) (B) p16^{INK4a+} cells (IHC), (C) cCasp3^{+} cells (IF) (D) Ki-67^{+} cells (IF) and (E) Sox10^{+} cells (IF). IF and IHC quantification of FFPE B16 section. *Cyp27a1*$^{\Delta Cx3cr1\text{-}Cre}$ (n = 5) *Cyp27a1*$^{fl/fl}$ (n = 5) **p < 0.01. ns. not significant. Data represents the mean.
(F) Representative IF image of Ki-67 staining.

3.7 No Change in Metabolism of Unstimulated Cultured Bone Marrow Derived Macrophages

To investigate whether 27-HC serves as a tumor-specific driver rather than a general metabolic regulator, we performed SCENITH™ assays (Argüello et al., 2020) on unstimulated BMDMs from *Cyp27a1*$^{\Delta Cx3cr1\text{-}Cre}$ and *Cyp27a1*$^{fl/fl}$. SCENITH™ measures translational inhibition under glycolysis (2-Deoxy-D-Glucose, DG) and OXPHOS (oligomycin A, O) blockade to infer metabolic reliance (Figure 12A)

First, we confirmed that glycolysis and oxidative phosphorylation were inhibited in cultured BMDMs (both *Cyp27a1*$^{\Delta Cx3cr1\text{-}Cre}$ and *Cyp27a1*$^{fl/fl}$) by DG and O, as shown by similar puromycin incorporation levels compared to uninhibited controls (Figure 12B). The combined DG and O treatment produced the highest inhibition (Figure 12B). Unstimulated *Cyp27a1*$^{\Delta Cx3cr1\text{-}Cre}$ and *Cyp27a1*$^{fl/fl}$ BMDMs showed no differences in glucose dependence, mitochondrial dependence, glycolytic capacity, or fatty acid/amino acid oxidation capacity (Figure 12C), indicating that unstimulated *Cyp27a1*$^{\Delta Cx3cr1\text{-}Cre}$ macrophages have an unchanged metabolism under steady-state conditions.

A

$$Glucose\ dependence\ (\%) = 100 * \left(\frac{Co - DG}{Co - DGO}\right)$$

$$Mitochondrial\ dependence\ (\%) = 100 * \left(\frac{Co - O}{Co - DGO}\right)$$

$$FAO\ \&\ AAO\ capacity\ (\%) = (100 - (100 * \left(\frac{Co - DG}{Co - DGO}\right)$$

$$Glycolytic\ capaity\ (\%) = (100 - (100 * \left(\frac{Co - O}{Co - DGO}\right)$$

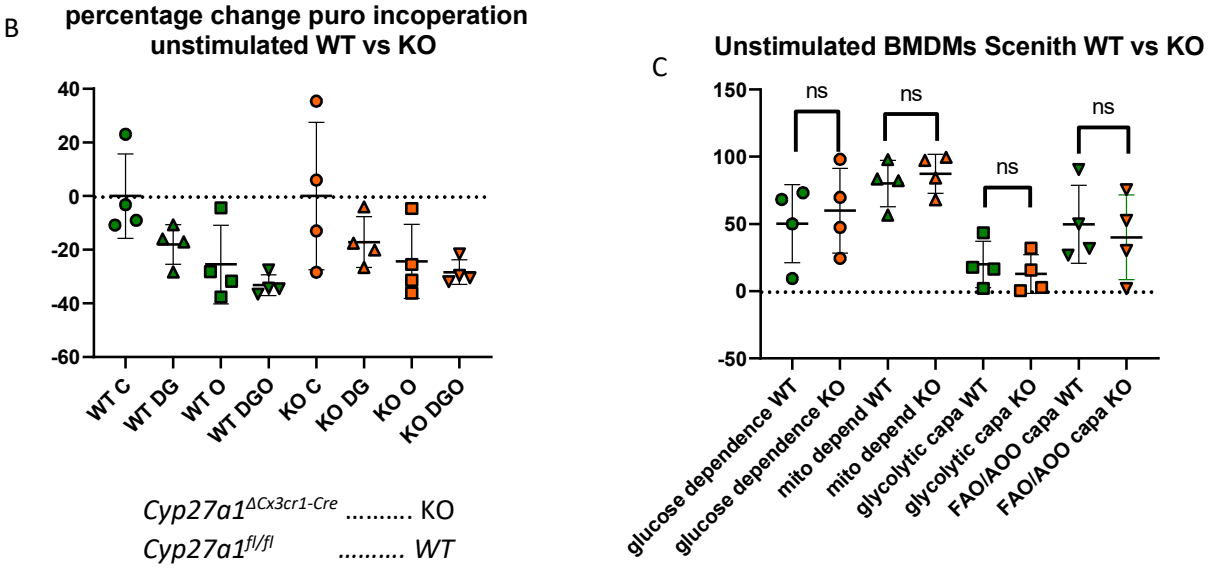

Figure 12. *Cyp27a1*$^{\Delta Cx3cr1\text{-}Cre}$ cultured BMDMs have an unchanged metabolism under steady stare conditions

(A) Formulas for calculation of glucose dependence, mitochondrial dependence, FAO & AAO capacity and glycolytic capacity.

(B) Puromycin incorporation change compared to DMSO control C, after DG, O, or DGO, treatment.

(C) Quantification of glucose dependency, mitochondrial dependency, glycolytic capacity and fatty acid oxidation capacity.

Cyp27a1$^{\Delta Cx3cr1\text{-}Cre}$ vs *Cyp27a1*$^{fl/fl}$ (n = 4/4). ns = non-significant. Data represents the mean with SD depicted.

3.8 IL4 Stimulated BMDMs do not fully Recapitulate *In Vivo* TME Markers

We next used flow cytometry to examine IL4 stimulated vs. unstimulated BMDMs for markers of activation and polarization. IL4 stimulated macrophages are described in literature to resemble M2-like polarization (Yunna et al., 2020). In addition to previously mentioned pro immunogenic signaling markers CD86 (Figure 13A), CD40 (Figure 13B) and MHCII (Figure 13C), scavenger receptor class B type I (CD36) expression was quantified due to its role in phagocytosis regulation (Fig 13D) (Fadok et al., 1998). TIM4 expression was quantified for its promotion of immune tolerance crosstalk with the lymphatic compartment (Fig 13C) (Wang et al., 2023). While CD11c was used as a general macrophage activation marker (Figure 13F) (Wu et al., 2009). Although IL4 treatment shifted all markers, no genotype differences emerged. (Figure 13). Notably, these *in vitro* results did not recapitulate the *vivo* differences (Figure 9), implying an incomplete model for TAMs.

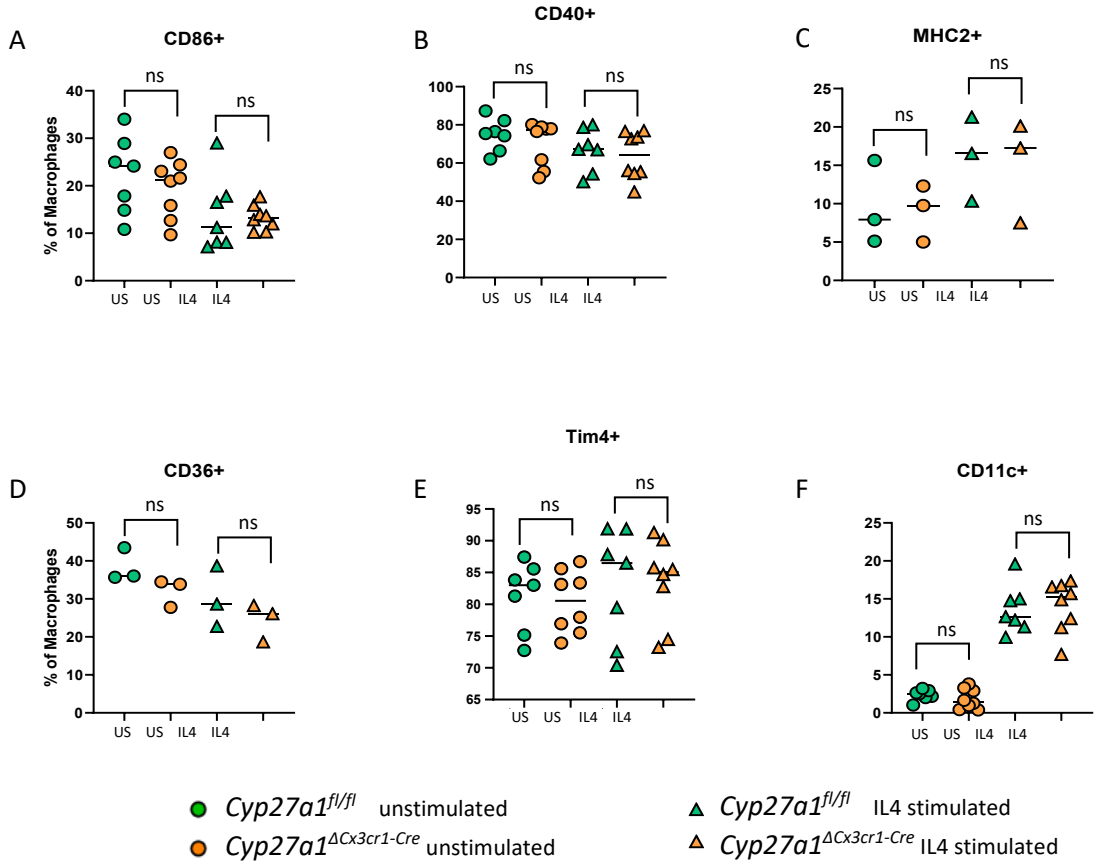

Figure 13. *In vitro* characterization of *Cyp27a1*$^{\Delta Cx3cr1\text{-}Cre}$ and *Cyp27a1*$^{fl/fl}$ BMDMs via flowcytometry based methodologies
(A, B, C, D, E, F) Characterization of (A) CD86, (B) CD40, (C) MHCII, (D) CD36, (E) Tim4

and (F) CD11c positive cells (as % of macrophages). *Cyp27a1*$^{fl/fl}$ and *Cyp27a1*$^{\Delta Cx3cr1\text{-}Cre}$BMDMs A, B, E, F n = 7; C, D n = 3. US = unstimulated, IL4 = IL4 stimulated (20ng/mL for 24 hours), ns = non-significant. Data represents the mean.

3.9 *In vitro* Cultured IL4 Stimulated *Cyp27a1*$^{\Delta Cx3cr1\text{-}Cre}$ Macrophages show Tendency for Increased Arginase 1 Production

We further used RT-qPCR to characterize our *Cyp27a1*$^{\Delta Cx3cr1\text{-}Cre}$ model *in vitro*. *Cyp27a1*$^{\Delta Cx3cr1\text{-}Cre}$ and *Cyp27a1*$^{fl/fl}$ macrophages were cultured unstimulated or stimulated with IL-4 for 24 hours to induce M2-like polarization (Yunna et al., 2020). As expected, *Cyp27a1* expression was significantly reduced in both unstimulated and IL-4–stimulated *Cyp27a1*$^{\Delta Cx3cr1\text{-}Cre}$ cells (Figure 14A). While IL-4 stimulation increased *mrc1* (CD206) expression, compared to unstimulated controls, there was no difference between *Cyp27a1*$^{\Delta Cx3cr1\text{-}Cre}$ and *Cyp27a1*$^{fl/fl}$ BMDMs (Figure 14B). IL-4 also reduced *Tnf-* α expression relative to unstimulated cells, but again no genotype difference was detected (Figure 14C). In contrast, *Arg1* was upregulated by IL-4 and showed a trend toward higher expression in *Cyp27a1*$^{\Delta Cx3cr1\text{-}Cre}$ (Figure 14D). *Arg1* expression in macrophages is reported to promote wound healing and dampens T cell activation by locally depleting L-arginine (Arlauckas et al., 2018).

Il10, *Nos2*, and *Angptl4* expression remained below reliable detection (Ct > 30) (Figures 14E, F, G). Il10 is classically induced by macrophages in response to microbial stimuli (Saraiva & Garra, 2010), *Nos2* encodes inducible nitric oxide synthases (iNOS) involved in pathogen clearance (Groves & Wang, 2000), and *Angptl4* is a PPAR-γ target implicated in lipid uptake (Ahmadian et al., 2013). All samples were normalized to *β-actin* levels.

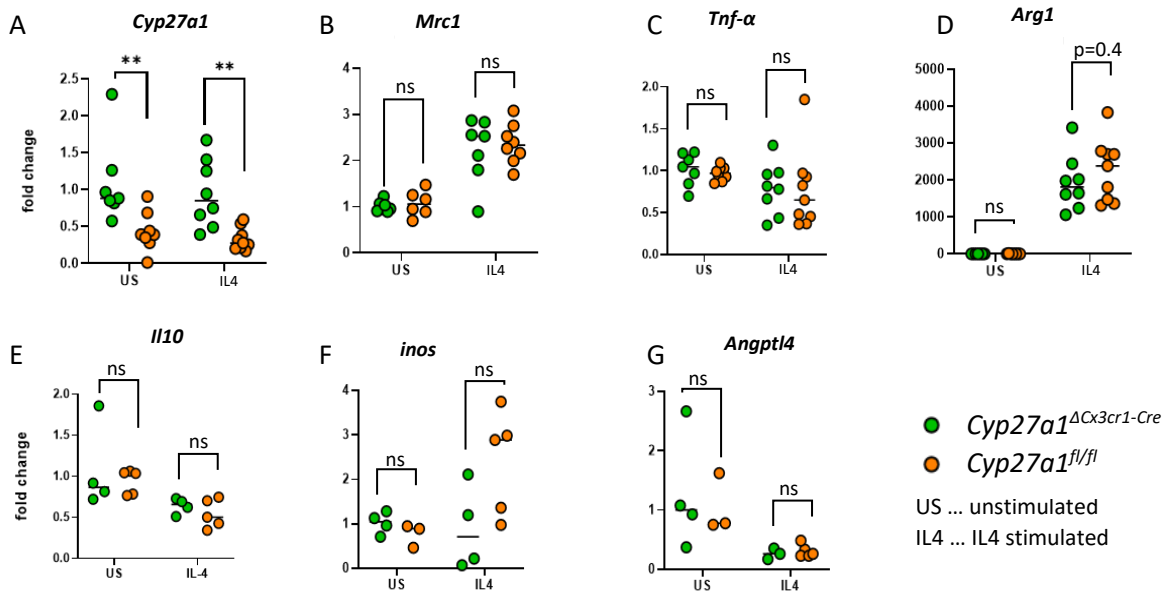

Figure 14. *In vitro* characterization of *Cyp27a1*$^{\Delta Cx3cr1\text{-}Cre}$ and *Cyp27a1*$^{fl/fl}$ BMDMs via RTqPCR (A, B, C, D, E, F, G) Fold change of (A) *Cyp27a1*, (B) *Mrc1*, (C) *Tnfα*, (D) *Arg1*, (E) *Il10*, (F) *Nos2* and (G) *Angptl4*, normalized to *β-actin* levels. BMDMs were stimulated with 20 nM IL4 for 24 h. *Cyp27a1*$^{fl/fl}$ vs *Cyp27a1*$^{\Delta Cx3cr1\text{-}Cre}$ (A, B, C, D n = 7/8) (E, F, G n=3/5). ns = non-significant. Data represents the mean.

3.10 *In vitro* Cultured B16 Supernatant Stimulated *Cyp27a1*$^{\Delta Cx3cr1\text{-}Cre}$ Macrophages show Tendency for Increased *Apoe* and *Abca1* Expression

Because M2-polarized macrophages do not necessarily reflect the *in vivo* behavior of TAMs (Xu et al., 2014) and based on our data from IL4-stimulated BMDMs (Figure 13), we reasoned that tumor-conditioned media (B16) would offer a more accurate approximation of TAMs (Fang et al., 2024). We continued investigating the lipid droplet dysregulation seen in BODIPY^{TM}493/507 assays (Figure 10) by examining lipid and fatty-acid metabolism drivers in *Cyp27a1*$^{\Delta Cx3cr1\text{-}Cre}$ and *Cyp27a1*$^{fl/fl}$ BMDMs. We focused on the expression of ATP-binding cassette transporters *Abcg8* and *Abca1*, which shuttle cholesterol and phospholipids (Su et al., 2002). *Abcg8* expression showed no change (Figure 15A), whereas *Abca1* trended slightly higher in *Cyp27a1*$^{\Delta Cx3cr1\text{-}Cre}$ under both conditions (Figure 15B). Expression of apolipoprotein (Apo) E mRNA, an important factor in lipoprotein clearance and metabolism (Civeira et al., 2024) was upregulated in both unstimulated and B16-conditioned BMDMs (Fig. 15C). We also measured *Nr1h3* (LXRα) and *Nr1h2* (LXRβ) mRNA levels, which code for TF involved in 27-

HC mediated regulation of lipid homeostasis (Hong and Tontonoz, 2014), but neither showed notable changes under any stimulus or genotype (Fig. 15D, E).

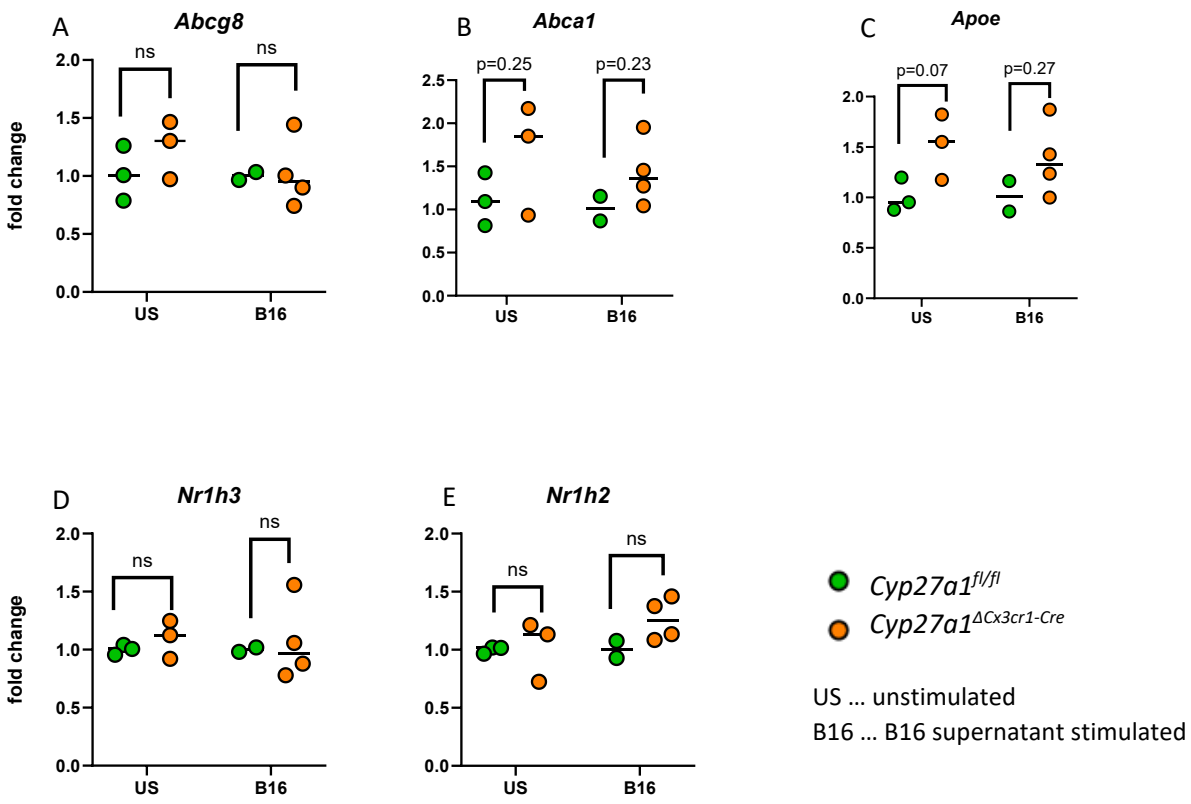

Figure 15. *In vitro* characterization of B16 supernatant stimulated *Cyp27a1*$^{\Delta Cx3cr1\text{-}Cre}$ and *Cyp27a1*$^{fl/fl}$ BMDMs via RTqPCR based methodologies
(A, B, C, D, E) Fold change of mRNA levels of (A) *Abcg8* (B) *Abca1*, (C) *Apoe*, (D) *Nr1h3* and (E) *Nr1h2* normalized to *β-actin*. *Cyp27a1*$^{\Delta Cx3cr1\text{-}Cre}$(n=2-3) and *Cyp27a1*$^{fl/fl}$ (n=3-4) BMDMs were stimulated with B16 supernatant for 24 h. ns = non-significant. Data represents the mean.

3.11 Phagocytic Capacity of *Cyp27a1*$^{\Delta Cx3cr1\text{-}Cre}$ Macrophages is Increased

Next, we investigated the role of macrophage-mediated phagocytosis in controlling tumor growth, as macrophages are key phagocytes and antigen-presenting cells (Li M. et al., 2023) Therefore, *Cyp27a1*$^{\Delta Cx3cr1\text{-}Cre}$ and *Cyp27a1*$^{fl/fl}$ were differentiated *in vitro* and co-cultured with CFSE-labeled B16 melanocytes for 3 hours. Phagocytic capacity, quantified by CFSE^{+} macrophages was significantly higher in *Cyp27a1*$^{\Delta Cx3cr1\text{-}Cre}$ than in *Cyp27a1*$^{fl/fl}$ (Figure 16). Because phagocytosis correlates with macrophage polarization and metabolism (Lesbats et al., 2025), lipid dysregulation in the *Cyp27a1*$^{\Delta Cx3cr1\text{-}Cre}$ model (Figure 10) may drive this increased phagocytic capacity.

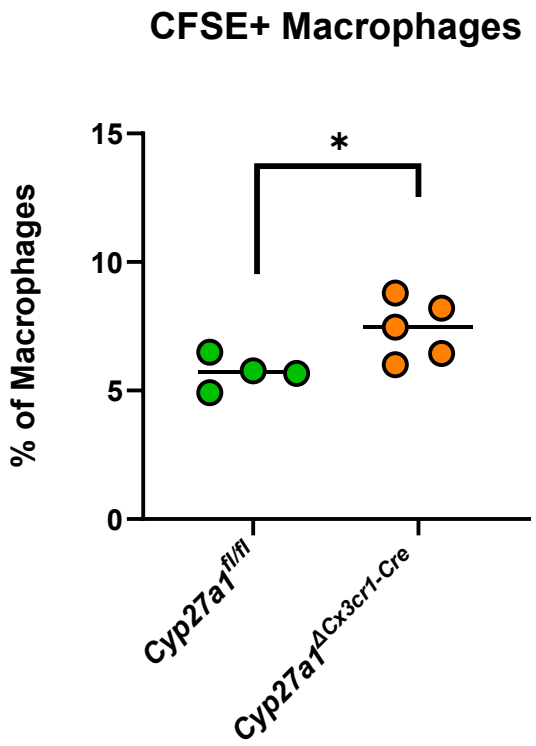

Figure 16. Evaluation of phagocytic capacity of *Cyp27a1*$^{\Delta Cx3cr1\text{-}Cre}$ and *Cyp27a1*$^{fl/fl}$ BMDMs

Scatter plot depicting the percentage of CFSE+ macrophages among total macrophages. *Cyp27a1*$^{fl/fl}$ (n=4) and *Cyp27a1*$^{\Delta Cx3cr1\text{-}Cre}$ (n=5) BMDMs co-cultured for 3 hours with CFSE+ B16 melanocytes. $p < 0.05$: *. Data represents the mean.

3.12 Confirmation of CYP27A1 Expression in Macrophages in Human Melanoma

Finally, we aimed to confirm the presence of CYP27A1 in human TAMs. In FFPE-preserved human melanoma samples, co-staining for the pan-macrophage marker CD68, CYP27A1, and DAPI confirmed CYP27A1 expression in macrophages. (Figure 17).

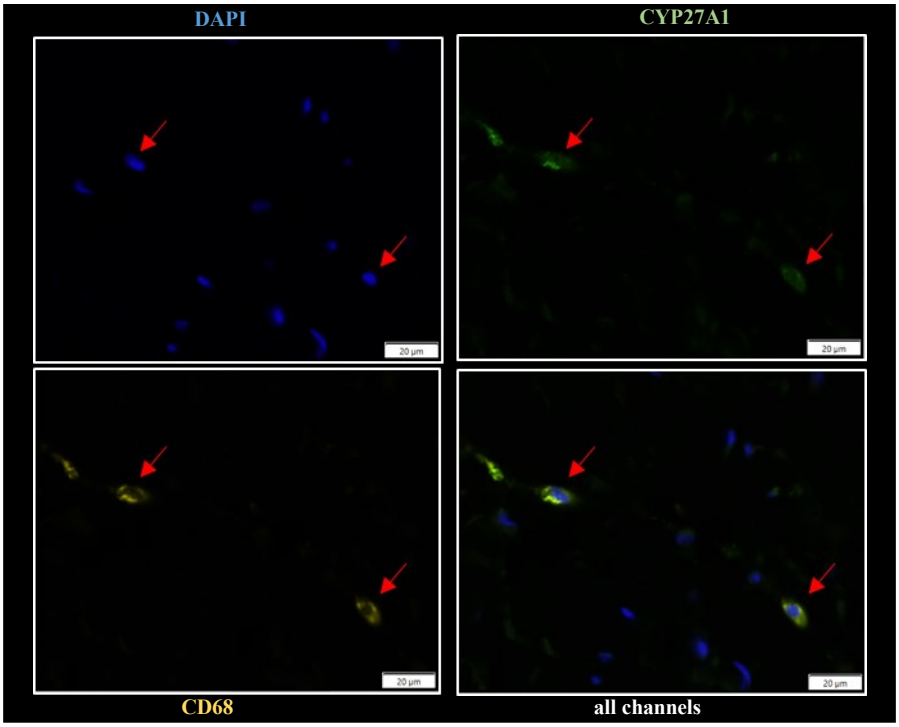

Figure 17. Confirmation CYP27A1 activity in human melanoma
Immunofluorescent images of FFPE human melanoma sections, stained for DAPI (top left), CYP27A1 (top right), CD68 (bottom left), and merged (bottom right). Scale bars = 20 µm. Red arrows highlight co-localized macrophages.

4. Discussion

Macrophages form a critical immune cell population involved in many cellular processes, including tissue homeostasis, and the immunogenic clearance of invading pathogens and tumors (Li et al., 2023). In order to fulfill such diverse functions, macrophages possess a high degree of cellular plasticity, an evolutionary perk that malignant tumors exploit, transforming macrophages into tumor-associated macrophages, an immune cell subpopulation characterized by its tumor-promoting effects (Ryan et al., 2020). Metabolic reprogramming and signaling within the TME are key factors driving this process (de Visser & Joyce, 2023). Therefore, the augmentation of macrophage functions in tumor settings represents a promising path for improving current cancer therapies.

In this thesis, we have presented evidence that macrophage-specific CYP27A1 activity, an enzyme involved in cholesterol metabolism, revealed direct involvement in the initial stages of tumor progression. We achieved targeted ablation by crossing *Cyp27a1*$^{fl/fl}$ mice with a *Cx3cr1-Cre* line, exploiting *Cx3cr1*'s predominant expression in macrophages (Imai et al., 1997). Despite the revolutionizing impact of the Cre–LoxP system in the biomedical field, its application is complicated by variable recombination efficiency, unreliability between reporter activation and complete gene excision, and reliance on limited amount of characterized cell-type–specific markers (Tian & Zhou, 2021). Accordingly, we validated CYP27A1 deletion at the genomic, transcript, and protein levels. However, because *Cx3cr1* is not exclusively expressed in macrophages and our Cre-mediated recombination efficiency was approximately 70–80% in BMDMs, these findings should be confirmed using an alternative macrophage-specific Cre driver. A strong candidate is *Lyz2-Cre* based mouse models, which utilizes the lysosome M locus expressed selectively in myelomonocytic cells such as monocytes, macrophages, and granulocytes and has been widely used to achieve macrophage specific gene deletions (Clausen et al., 1999; Shi et al., 2019; Fritsch et al., 2023).

Macrophage-restricted deletion of CYP27A1 reveals its pivotal role in driving tumor growth in both melanoma and colon adenocarcinoma models. Tumors in *Cyp27a1*$^{\Delta Cx3cr1\text{-}Cre}$ mice were significantly delayed in entering an exponential growth phase. These growth-deficient tumors also exhibited no detectable difference in their adaptive immune cell compartment when compared to their respective controls. An unexpected finding considering previous reports from Yan et al. (2023) which observed T cell exhaustion in a 27-HC-enriched TME, with 27-HC being the main metabolite produced by CYP27A1. Thus, an important next step in this project

is to evaluate the 27-HC concentrations in the TME of the two cancer models used in this thesis; until then, it remains unclear whether local 27-HC concentrations are reduced.

Furthermore, various cancer cells, including melanoma cells, have been shown, at least on a scRNA sequencing level, to have *Cyp27a1* activity (Jerby-Arnon et al., 2018). In addition to cancer cells, *Cyp27a1* activity in the TME has also been attributed to cancer-associated fibroblasts and endothelial cells (Jerby-Arnon et al., 2018). Therefore, it could be argued that macrophage-derived CYP27A1 activity alone may be insufficient to alter 27-HC TME concentrations enough to significantly impact adaptive immune cell populations, to the degree observed by others. Hence, these results indicate that the observed tumor growth deficiency is primary a macrophage-driven phenotype. Our observations of the TME macrophage compartment revealed an overall reduction in macrophage numbers further supporting this notion.

However, it is also important to note that CYP27A1 activity could potentially influence cancer growth in 27-HC-independent ways. In addition to its role in 27-HC production, CYP27A1 also has 25-hydroxylase functionality and converts cholecalciferol into calcidiol, an intermediate step in the vitamin D pathway (Bikle, 2014). Additionally, it is involved in the conversion of lumisterol$_3$ and tachysterol$_3$ into their respective hydroxy metabolites, which have been reported to enhance skin protection against oxidative stress and DNA damage potentially providing protection against excessive cellular stress in cancer settings (Slominski et al., 2024). Furthermore, given the numerous unresolved questions in the field of oxysterols, the possibility of yet unidentified pathways and interactions should be carefully considered.

The evidence for macrophage involvement in various stages of tumor progression is staggering (Li et al., 2023); however, the exact role they play at distinct phases of tumor development remains somewhat unclear. Nonetheless, evidence points toward a “two-fold” function, in which, during tumor initiation and early stages of tumor progression, macrophages foster a pro-inflammatory environment, which is mutagenic and supports growth (Salmaninejad et al., 2019), while in later malignant tumor stages, TAMs promote angiogenesis, enhance tumor cell migration and invasion, and suppress anti-tumor immunity (Qian & Pollard, 2010). In our melanoma mouse model, the macrophage compartment of *Cyp27a1*$^{\Delta Cx3cr1\text{-}Cre}$ tumors was overall smaller, with indications of reduced expression of both “M1” (CD40, CD86) and “M2” (CD206) -like receptors, despite the smaller tumor volumes. Thus, it appears that *Cyp27a1*$^{\Delta Cx3cr1\text{-}Cre}$ macrophages are either quantitatively (fewer overall macrophages) and/or qualitatively (fewer populations expressing effector receptors) incapable of eliciting tumor-

promoting functions comparable to those of *Cyp27a1*$^{fl/fl}$ macrophages. Further *in vitro* characterization of TAM-polarized BMDMs for the expression of various macrophage effector markers could provide additional insight into the underlying mechanisms. Taken together, these findings underscore the importance of macrophage metabolism and its function within the TME while highlighting the need for a comprehensive understanding of all cellular interactions in the TME. Additional characterization with TAM polarized in vitro BMDMs regarding the expression of varies effector markers is a potential avenue in order to gain further insight into the underlying affected mechanisam.

For cancer to grow at an exponential rate, it requires a substantial supply of cellular building blocks. Cancer often reprograms the local TME, leading to an increase in lipids, that serve both as essential building blocks for membranes and as fuel for energy-driven processes (Butler et al., 2020). In this context, our data indicate an overall increased lipid droplet load in the growth-deficient tumors of *Cyp27a1*$^{\Delta Cx3cr1\text{-}Cre}$ mice, which is an unexpected finding. Moreover, *Cyp27a1*$^{\Delta Cx3cr1\text{-}Cre}$ mice also exhibited a higher percentage of cells that were positive for Ki-67, a marker of cell proliferation. These cellular states are associated with tumor expansion in the literature (Li et al., 2015; Butler et al., 2020). One observation worth considering here is that the tumors were obtained 12 days after inoculation, which was the first time point at which a significant divergence between *Cyp27a1*$^{\Delta Cx3cr1\text{-}Cre}$ and *Cyp27a1*$^{fl/fl}$ was observed. But, in this case, the tumors in the *Cyp27a1*$^{\Delta Cx3cr1\text{-}Cre}$ mice had already undergone an increased number of cellular divisions, using up lipid droplets either as an energy source or as a building block. Meanwhile, *Ki-67* expression is under strict regulation in cells and is degraded via the APC/C-Cdh1 complex after ubiquitination during G1 phase (Sun & Kaufmann, 2018). Additionally, Ki-67 levels accumulate continually during S and G2 and peak during the M phase (Miller et al., 2018). Therefore, a potential explanation for the observed growth-deficient tumor phenotype (despite increased Ki-67 levels in our *Cyp27a1*$^{\Delta Cx3cr1\text{-}Cre}$ mice) could be a decrease in the speed at which the tumor cell passes cell cycle checkpoints, thereby allowing for more Ki-67 accumulation. In further studies, this question could perhaps be answered via an evaluation of tumor sections obtained from earlier time points (day 6/7 after inoculation), when the overall tumor volume between *Cyp27a1*$^{\Delta Cx3cr1\text{-}Cre}$ and *Cyp27a1*$^{fl/fl}$ is still equal.

Another interesting finding in our macrophage-specific knockout model was an observed increase in phagocytic capacity of *in vitro* cultivated BMDMs. Although the enhanced phagocytosis of *Cyp27a1*$^{\Delta Cx3cr1\text{-}Cre}$ macrophages aligns with the overall trend of reduced tumor volume in this model, it remains debatable whether this effect alone is sufficient to explain the

reduction in tumor growth. Macrophages represent the most important phagocytes *in vivo* and engage in engulfing cancer cells, aging or abnormal cells, damaged or apoptotic cells, as well as cellular debris (DeNardo & Ruffell, 2019). TAMs in solid tumor settings have a reduced phagocytic capacity, generally attributed to inhibitory receptor ligand interactions facilitating "don't eat me signals" such as CD47–SIRPα or PD-1/PD-L1 interactions (Pan et al., 2020). Although disruption of these interactions, often through antibody mediated blockage of the receptors, can restore phagocytic capacity. (Pan et al., 2020). In addition, metabolic repolarization of macrophages toward enhancing anti-tumor clearance is actively pursued by many laboratories and seen as a promising adjunct to anticancer therapies (Saha et al., 2024). Even further, chimeric antigen receptor (CAR) macrophages have recently undergone the first-ever phase 1 trials in humans (Reiss et al., 2025), although with mixed results regarding their tumor clearance efficiency. This highlights the importance of understanding the TME and the complexity of cellular interactions within it to improve solid tumor therapies. Our data indicates that cholesterol metabolism is involved in the phagocytic capacity of macrophages, at least under *in vitro* conditions. In macrophages, increased lipid synthesis via the mTOR pathway leading to elevated SREBP1α activity has been shown to enhance phagocytic capacity (Lee et al., 2018). Overall, lipid metabolism plays roles in many macrophage effector functions, from phagocytosis to immune signaling and cytokine production (Yan & Horng, 2020). Metabolic reprogramming in macrophages through the disruption of cholesterol catabolism via CYP27A1 deficiency could therefore shift their polarization toward increased phagocytosis. In addition, our measurements indicate an increase in LD content within the macrophages themselves. LDs in macrophages could provide a reservoir of phospholipids that can then be utilized during membrane protrusion and phagocytic engulfment (Chandak et al., 2010; Yan & Horng, 2020). However, to further validate our *in vitro* findings, macrophage phagocytic activity should next be evaluated in an *in vivo* setting.

Finally, our findings also support the presence of CYP27A1 activity in human macrophages within solid tumor settings. This offers new insights into potential alternative applications of CYP27A1 inhibitors as cancer therapies. Notably, this approach could accelerate translation into human clinical trials, given that FDA approved antihypertensive drugs, such as felodipine and nilvadipine, are known to inhibit CYP27A1 function based on their 1,4 dihydropyridine core (Lam et al., 2018). These compounds represent a promising opportunity for augmenting future cancer treatments; however, further research is needed to elucidate the precise role of CYP27A1 across different tumor settings and its effect on the TME.

Overall, our findings describe a novel dimension of tumor-immune interaction in which CYP27A1 activity in macrophages within the TME supports tumor growth via metabolic reprogramming of both tumor and immune cells. Although a definitive explanation of the underlying mechanisms was not achieved during this thesis, considerable progress has been made. Our results underscore the importance of macrophages in the early stages of tumor initiation and progression and highlight the need for a comprehensive understanding of the interactions among all cell populations within the TME.

5. Abstract

5.1. English

Cancer remains a global health challenge, ranking as the second leading cause of death worldwide with nearly 10 million fatalities in 2020. Although immunotherapies like immune checkpoint blockade have improved outcomes in some patients, response rates in solid tumors seldom exceed 40%, highlighting the pivotal role of the tumor microenvironment (TME) in driving disease progression and resistance. The cholesterol metabolite 27-hydroxycholesterol (27-HC) has recently emerged as a critical oncometabolite that fosters both primary and metastatic tumor growth by dampening immune cell function. Single-cell RNA sequencing has identified tumor-associated macrophages as the predominant non-malignant source of CYP27A1, the enzyme responsible for 27-HC synthesis within the TME.

In this thesis, we investigate the contribution of macrophage-derived CYP27A1 to tumor progression using murine melanoma and colorectal cancer models. We generated macrophage-specific knockout mice (*Cyp27a1*$^{\Delta Cx3cr1\text{-}Cre}$) to ablate CYP27A1 selectively in myeloid cells. In both models, *Cyp27a1*$^{\Delta Cx3cr1\text{-}Cre}$ mice displayed significantly reduced tumor volumes and prolonged survival relative to wild-type controls. Immunohistochemical analysis of tumor sections revealed increased lipid droplet accumulation in *Cyp27a1*$^{\Delta Cx3cr1\text{-}Cre}$ tumors, indicative of metabolic reprogramming. Complementary *in vitro* assays showed that CYP27A1-deficient macrophages exhibit enhanced phagocytic capacity compared to their wild-type counterparts. Finally, analysis of human solid tumor specimens confirmed CYP27A1 activity within tumor-associated macrophages.

Collectively, these findings establish macrophage-derived CYP27A1 as a key driver of a tumor-promoting microenvironment through metabolic modulation. They also identify CYP27A1 inhibition as a promising therapeutic strategy to bolster anti-tumor immunity in solid cancers, underscoring the critical importance of cholesterol metabolism within the TME.

5.2. Deutsch

Krebs ist nach wie vor eine globale Gesundheitsherausforderung und mit fast 10 Millionen Todesfällen im Jahr 2020 die zweithäufigste Todesursache weltweit. Obwohl Immuntherapien wie die Immun-Checkpoint-Blockade bei einigen Patientinnen und Patienten zu besseren Ergebnissen geführt haben, liegen die Ansprechraten bei soliden Tumoren selten über 40 %, was die entscheidende Rolle der Tumormikroumgebung (TMU) bei der Förderung des Krankheitsverlaufs und der Resistenz unterstreicht. Der Cholesterinmetabolit 27-Hydroxycholesterin (27-HC) hat sich kürzlich als kritischer Onkometabolit herausgestellt, der sowohl das Wachstum von Primärtumoren als auch von Metastasen fördert, indem er die Funktion der Immunzellen dämpft. Durch Einzelzell-RNA-Sequenzierung wurden tumorassoziierte Makrophagen als die vorherrschende nicht-maligne Quelle von CYP27A1 identifiziert, dem Enzym, das für die 27-HC-Synthese innerhalb der TMU verantwortlich ist.

In dieser Arbeit untersuchen wir den Beitrag von Makrophagen-abgeleitetem CYP27A1 zur Tumorprogression anhand von Mausmodellen für Melanome und Darmkrebs. Wir haben Makrophagen-spezifische Knockout-Mäuse (*Cyp27a1*$^{\Delta Cx3cr1\text{-}Cre}$) erzeugt, um CYP27A1 selektiv in myeloischen Zellen zu entfernen. In beiden Modellen zeigten *Cyp27a1*$^{\Delta Cx3cr1\text{-}Cre}$ Mäuse im Vergleich zu Wildtyp-Kontrollen ein signifikant reduziertes Tumorvolumen und eine verlängerte Überlebenszeit. Die immunhistochemische Analyse von Tumorschnitten zeigte eine erhöhte Ansammlung von Lipidtröpfchen in *Cyp27a1*$^{\Delta Cx3cr1\text{-}Cre}$ Tumoren, was auf eine metabolische Umprogrammierung hindeutet. Ergänzende *In-vitro* Assays zeigten, dass CYP27A1-defiziente Makrophagen im Vergleich zu ihren Wildtyp-Gegenstücken eine erhöhte Phagozytose Fähigkeit aufweisen. Schließlich bestätigte die Analyse von menschlichen soliden Tumorgewebeproben die Aktivität von CYP27A1 in tumorassoziierten Makrophagen.

Zusammengenommen belegen diese Ergebnisse, dass aus Makrophagen stammendes CYP27A1 durch metabolische Modulation eine wichtige Rolle bei der Förderung einer tumorfördernden Mikroumgebung spielt. Sie identifizieren außerdem die Hemmung von CYP27A1 als vielversprechende therapeutische Strategie zur Stärkung der Anti-Tumor-Immunität bei soliden Tumoren und unterstreichen damit die entscheidende Bedeutung des Cholesterinstoffwechsels innerhalb der TMU.

6. Literature

1. van Reyk, D. M., Brown, A. J., Hult'en, L. M., Dean, R. T., & Jessup, W. (2006). Oxysterols in biological systems: sources, metabolism and pathophysiological relevance. *Redox report: communications in free radical research*, *11*(6), 255–262. https://doi.org/10.1179/135100006X155003
2. Abdalkareem Jasim, S., Kzar, H. H., Haider Hamad, M., Ahmad, I., Al-Gazally, M. E., Ziyadullaev, S., Sivaraman, R., Abed Jawad, M., Thaeer Hammid, A., Oudaha, K. H., Karampoor, S., & Mirzaei, R. (2022). The emerging role of 27-hydroxycholesterol in cancer development and progression: An update. *International immunopharmacology*, *110*, 109074. https://doi.org/10.1016/j.intimp.2022.109074
3. Aderem, A., & Underhill, D. M. (1999). Mechanisms of phagocytosis in macrophages. *Annual review of immunology*, *17*, 593–623. https://doi.org/10.1146/annurev.immunol.17.1.593
4. Afonina, I. S., Cullen, S. P., & Martin, S. J. (2010). Cytotoxic and non-cytotoxic roles of the CTL/NK protease granzyme B. *Immunological reviews*, *235*(1), 105–116. https://doi.org/10.1111/j.0105-2896.2010.00908.x
5. Ahmadian, M., Suh, J. M., Hah, N., Liddle, C., Atkins, A. R., Downes, M., & Evans, R. M. (2013). PPARγ signaling and metabolism: the good, the bad and the future. *Nature medicine*, *19*(5), 557–566. https://doi.org/10.1038/nm.3159
6. Amersfoort, J., Eelen, G., & Carmeliet, P. (2022). Immunomodulation by endothelial cells - partnering up with the immune system?. *Nature reviews. Immunology*, *22*(9), 576–588. https://doi.org/10.1038/s41577-022-00694-4
7. Argüello, R. J., Combes, A. J., Char, R., Gigan, J. P., Baaziz, A. I., Bousiquot, E., Camosseto, V., Samad, B., Tsui, J., Yan, P., Boissonneau, S., Figarella-Branger, D., Gatti, E., Tabouret, E., Krummel, M. F., & Pierre, P. (2020). SCENITH: A Flow Cytometry-Based Method to Functionally Profile Energy Metabolism with Single-Cell Resolution. *Cell metabolism*, *32*(6), 1063–1075.e7. https://doi.org/10.1016/j.cmet.2020.11.007
8. Arlauckas, S. P., Garren, S. B., Garris, C. S., Kohler, R. H., Oh, J., Pittet, M. J., & Weissleder, R. (2018). Arg1 expression defines immunosuppressive subsets of tumor-associated macrophages. *Theranostics*, *8*(21), 5842–5854. https://doi.org/10.7150/thno.26888
9. Baker S. G. (2014). A cancer theory kerfuffle can lead to new lines of research. *Journal of the National Cancer Institute*, *107*(2), dju405. https://doi.org/10.1093/jnci/dju405
10. Bauman, D. R., Bitmansour, A. D., McDonald, J. G., Thompson, B. M., Liang, G., & Russell, D. W. (2009). 25-Hydroxycholesterol secreted by macrophages in response to Toll-like receptor activation suppresses immunoglobulin A production. *Proceedings of the National Academy of Sciences of the United States of America*, *106*(39), 16764–16769. https://doi.org/10.1073/pnas.0909142106
11. Bi, K., He, M. X., Bakouny, Z., Kanodia, A., Napolitano, S., Wu, J., Grimaldi, G., Braun, D. A., Cuoco, M. S., Mayorga, A., DelloStritto, L., Bouchard, G., Steinharter, J., Tewari, A. K., Vokes, N. I., Shannon, E., Sun, M., Park, J., Chang, S. L., McGregor, B. A., … Van Allen, E. M. (2021). Tumor and immune reprogramming during immunotherapy in advanced renal cell carcinoma. *Cancer cell*, *39*(5), 649–661.e5. https://doi.org/10.1016/j.ccell.2021.02.015

12. Biasi, F., Leoni, V., Gamba, P., Sassi, K., Lizard, G., & Poli, G. (2022). Role of 27-hydroxycholesterol and its metabolism in cancer progression: Human studies. *Biochemical pharmacology*, *196*, 114618. https://doi.org/10.1016/j.bcp.2021.114618
13. Bied, M., Ho, W. W., Ginhoux, F., & Blériot, C. (2023). Roles of macrophages in tumor development: a spatiotemporal perspective. *Cellular & molecular immunology*, *20*(9), 983–992. https://doi.org/10.1038/s41423-023-01061-6
14. Bikle D. D. (2014). Vitamin D metabolism, mechanism of action, and clinical applications. *Chemistry & biology*, *21*(3), 319–329. https://doi.org/10.1016/j.chembiol.2013.12.016
15. Bjerre, L. M., & LeLorier, J. (2001). Do statins cause cancer? A meta-analysis of large randomized clinical trials. *The American journal of medicine*, *110*(9), 716–723. https://doi.org/10.1016/s0002-9343(01)00705-7
16. Brücher, B. L., & Jamall, I. S. (2016). Somatic Mutation Theory - Why it's Wrong for Most Cancers. *Cellular physiology and biochemistry: international journal of experimental cellular physiology, biochemistry, and pharmacology*, *38*(5), 1663–1680. https://doi.org/10.1159/000443106
17. Butler, L. M., Perone, Y., Dehairs, J., Lupien, L. E., de Laat, V., Talebi, A., Loda, M., Kinlaw, W. B., & Swinnen, J. V. (2020). Lipids and cancer: Emerging roles in pathogenesis, diagnosis and therapeutic intervention. *Advanced drug delivery reviews*, *159*, 245–293. https://doi.org/10.1016/j.addr.2020.07.013
18. Cavaillon J. M. (2011). The historical milestones in the understanding of leukocyte biology initiated by Elie Metchnikoff. *Journal of leukocyte biology*, *90*(3), 413–424. https://doi.org/10.1189/jlb.0211094
19. Chen, T., Xu, Z. G., Luo, J., Manne, R. K., Wang, Z., Hsu, C. C., Pan, B. S., Cai, Z., Tsai, P. J., Tsai, Y. S., Chen, Z. Z., Li, H. Y., & Lin, H. K. (2023). NSUN2 is a glucose sensor suppressing cGAS/STING to maintain tumorigenesis and immunotherapy resistance. *Cell metabolism*, *35*(10), 1782–1798.e8. https://doi.org/10.1016/j.cmet.2023.07.009
20. Cheng C, Geng F, Cheng X, Guo D. Lipid metabolism reprogramming and its potential targets in cancer. Cancer Commun (Lond). 2018 May 21;38(1):27. doi: 10.1186/s40880-018-0301-4. PMID: 29784041; PMCID: PMC5993136.
21. Civeira, F., Martín, C., & Cenarro, A. (2024). APOE and familial hypercholesterolemia. *Current opinion in lipidology*, *35*(4), 195–199. https://doi.org/10.1097/MOL.0000000000000937
22. Clausen, B. E., Burkhardt, C., Reith, W., Renkawitz, R., & Förster, I. (1999). Conditional gene targeting in macrophages and granulocytes using LysMcre mice. *Transgenic research*, *8*(4), 265–277. https://doi.org/10.1023/a:1008942828960
23. Czech M. P. (2000). PIP2 and PIP3: complex roles at the cell surface. *Cell*, *100*(6), 603–606. https://doi.org/10.1016/s0092-8674(00)80696-0
24. Dang, Q., Li, B., Jin, B., Ye, Z., Lou, X., Wang, T., Wang, Y., Pan, X., Hu, Q., Li, Z., Ji, S., Zhou, C., Yu, X., Qinv, Y., & Xu, X. (2024). Cancer immunometabolism: advent, challenges, and perspective. *Molecular cancer*, *23*(1), 72. https://doi.org/10.1186/s12943-024-01981-5
25. de Visser, K. E., & Joyce, J. A. (2023). The evolving tumor microenvironment: From cancer initiation to metastatic outgrowth. *Cancer cell*, *41*(3), 374–403. https://doi.org/10.1016/j.ccell.2023.02.016
26. DeNardo, D. G., & Ruffell, B. (2019). Macrophages as regulators of tumour immunity and immunotherapy. *Nature reviews. Immunology*, *19*(6), 369–382. https://doi.org/10.1038/s41577-019-0127-6

27. Duesberg, P., Mandrioli, D., McCormack, A., & Nicholson, J. M. (2011). Is carcinogenesis a form of speciation?. *Cell cycle (Georgetown, Tex.)*, *10*(13), 2100–2114. https://doi.org/10.4161/cc.10.13.16352
28. Fang X, Wu Y, Qin H, Zhao P, Shan M, Wang F, Li Q. Protocol for building an in vitro model of M2-like tumor-associated macrophages with lactic acid or conditioned medium from Lewis cells. STAR Protoc. 2024 Jun 21;5(2):103120. doi: 10.1016/j.xpro.2024.103120. Epub 2024 Jun 9. PMID: 38857154; PMCID: PMC11193043.
29. Fadok, V. A., Warner, M. L., Bratton, D. L., & Henson, P. M. (1998). CD36 is required for phagocytosis of apoptotic cells by human macrophages that use either a phosphatidylserine receptor or the vitronectin receptor (alpha v beta 3). *Journal of immunology (Baltimore, Md.: 1950)*, *161*(11), 6250–6257.
30. Fritsch, S. D., Sukhbaatar, N., Gonzales, K., Sahu, A., Tran, L., Vogel, A., Mazic, M., Wilson, J. L., Forisch, S., Mayr, H., Oberle, R., Weiszmann, J., Brenner, M., Vanhoutte, R., Hofmann, M., Pirnes-Karhu, S., Magnes, C., Kühnast, T., Weckwerth, W., Bock, C., … Weichhart, T. (2023). Metabolic support by macrophages sustains colonic epithelial homeostasis. *Cell metabolism*, *35*(11), 1931–1943.e8. https://doi.org/10.1016/j.cmet.2023.09.010
31. Galdiero, M. R., Bonavita, E., Barajon, I., Garlanda, C., Mantovani, A., & Jaillon, S. (2013). Tumor associated macrophages and neutrophils in cancer. *Immunobiology*, *218*(11), 1402–1410. https://doi.org/10.1016/j.imbio.2013.06.003
32. García-Sastre, A., Stanley, E. R., Ginhoux, F., Frenette, P. S., … Merad, M. (2013). Tissue-resident macrophages self-maintain locally throughout adult life with minimal contribution from circulating monocytes. *Immunity*, *38*(4), 792–804. https://doi.org/10.1016/j.immuni.2013.04.004
33. Ginhoux, F., Greter, M., Leboeuf, M., Nandi, S., See, P., Gokhan, S., Mehler, M. F., Conway, S. J., Ng, L. G., Stanley, E. R., Samokhvalov, I. M., & Merad, M. (2010). Fate mapping analysis reveals that adult microglia derive from primitive macrophages. *Science (New York, N.Y.)*, *330*(6005), 841–845. https://doi.org/10.1126/science.1194637
34. Goodman, S. R. (2008). Cell Membranes. In *Medical cell biology* (3rd ed., pp. 27-57).
35. Grewal, I. S., & Flavell, R. A. (1998). CD40 and CD154 in cell-mediated immunity. *Annual review of immunology*, *16*, 111–135. https://doi.org/10.1146/annurev.immunol.16.1.111
36. Griffiths, W. J., & Wang, Y. (2019). Oxysterol research: a brief review. *Biochemical Society transactions*, *47*(2), 517–526. https://doi.org/10.1042/BST20180135
37. Groves, J. T., & Wang, C. C. (2000). Nitric oxide synthase: models and mechanisms. *Current opinion in chemical biology*, *4*(6), 687–695. https://doi.org/10.1016/s1367-5931(00)00146-0
38. Guerra, L., Bonetti, L., & Brenner, D. (2020). Metabolic Modulation of Immunity: A New Concept in Cancer Immunotherapy. *Cell reports*, *32*(1), 107848. https://doi.org/10.1016/j.celrep.2020.107848
39. Habib, S., Osborn, G., Willsmore, Z., Chew, M. W., Jakubow, S., Fitzpatrick, A., Wu, Y., Sinha, K., Lloyd-Hughes, H., Geh, J. L. C., MacKenzie-Ross, A. D., Whittaker, S., Sanz-Moreno, V., Lacy, K. E., Karagiannis, S. N., & Adams, R. (2024). Tumor associated macrophages as key contributors and targets in current and future therapies for melanoma. *Expert review of clinical immunology*, *20*(8), 895–911. https://doi.org/10.1080/1744666X.2024.2326626
40. Hanselmann, R. G., & Welter, C. (2016). Origin of Cancer: An Information, Energy, and Matter Disease. *Frontiers in cell and developmental biology*, *4*, 121. https://doi.org/10.3389/fcell.2016.00121

41. Hong C, Tontonoz P. Liver X receptors in lipid metabolism: opportunities for drug discovery. Nat Rev Drug Discov. 2014 Jun;13(6):433-44. doi: 10.1038/nrd4280. Epub 2014 May 16. PMID: 24833295.
42. Hargadon, K. M., Johnson, C. E., & Williams, C. J. (2018). Immune checkpoint blockade therapy for cancer: An overview of FDA-approved immune checkpoint inhibitors. *International immunopharmacology*, *62*, 29–39. https://doi.org/10.1016/j.intimp.2018.06.001
43. Houslay M. D. (1985). Regulation of adenylate cyclase (EC 4.6.I.I) activity by its lipid environment. *The Proceedings of the Nutrition Society*, *44*(2), 157–165. https://doi.org/10.1079/pns19850034
44. Imai, T., Hieshima, K., Haskell, C., Baba, M., Nagira, M., Nishimura, M., Kakizaki, M., Takagi, S., Nomiyama, H., Schall, T. J., & Yoshie, O. (1997). Identification and molecular characterization of fractalkine receptor CX3CR1, which mediates both leukocyte migration and adhesion. *Cell*, *91*(4), 521–530. https://doi.org/10.1016/s0092-8674(00)80438-9
45. Jerby-Arnon, L., Shah, P., Cuoco, M. S., Rodman, C., Su, M. J., Melms, J. C., Leeson, R., Kanodia, A., Mei, S., Lin, J. R., Wang, S., Rabasha, B., Liu, D., Zhang, G., Margolais, C., Ashenberg, O., Ott, P. A., Buchbinder, E. I., Haq, R., Hodi, F. S., … Regev, A. (2018). A Cancer Cell Program Promotes T cell Exclusion and Resistance to Checkpoint Blockade. *Cell*, *175*(4), 984–997.e24. https://doi.org/10.1016/j.cell.2018.09.006
46. Jia, D., Chen, S., Bai, P., Luo, C., Liu, J., Sun, A., & Ge, J. (2022). Cardiac Resident Macrophage-Derived Legumain Improves Cardiac Repair by Promoting Clearance and Degradation of Apoptotic Cardiomyocytes After Myocardial Infarction. *Circulation*, *145*(20), 1542–1556. https://doi.org/10.1161/CIRCULATIONAHA.121.057549
47. Jia, D., Chen, S., Bai, P., Luo, C., Liu, J., Sun, A., & Ge, J. (2022). Cardiac Resident Macrophage-Derived Legumain Improves Cardiac Repair by Promoting Clearance and Degradation of Apoptotic Cardiomyocytes After Myocardial Infarction. *Circulation*, *145*(20), 1542–1556. https://doi.org/10.1161/CIRCULATIONAHA.121.057549
48. Jin, Y., Tan, Y., Wu, J., & Ren, Z. (2023). Lipid droplets: a cellular organelle vital in cancer cells. *Cell death discovery*, *9*(1), 254. https://doi.org/10.1038/s41420-023-01493-z
49. Kalluri R. (2016). The biology and function of fibroblasts in cancer. *Nature reviews. Cancer*, *16*(9), 582–598. https://doi.org/10.1038/nrc.2016.73
50. Kim, D., Lee, K. M., Lee, C., Jo, Y. S., Muradillaevna, M. S., Kim, J. H., Yoon, J. H., & Song, P. (2022). Pathophysiological role of 27-hydroxycholesterol in human diseases. *Advances in biological regulation*, *83*, 100837. https://doi.org/10.1016/j.jbior.2021.100837
51. Kim, H. J., Park, J. H., Kim, H. C., Kim, C. W., Kang, I., & Lee, H. K. (2022). Blood monocyte-derived $CD169^{+}$ macrophages contribute to antitumor immunity against glioblastoma. *Nature communications*, *13*(1), 6211. https://doi.org/10.1038/s41467-022-34001-5
52. Kimbung, S., Inasu, M., Stålhammar, T., Nodin, B., Elebro, K., Tryggvadottir, H., Ygland Rödström, M., Jirström, K., Isaksson, K., Jernström, H., & Borgquist, S. (2020). CYP27A1 expression is associated with risk of late lethal estrogen receptor-positive breast cancer in postmenopausal patients. Breast cancer research : BCR, 22(1), 123. https://doi.org/10.1186/s13058-020-01347-x
53. Kutlesa, S., Wessels, J. T., Speiser, A., Steiert, I., Müller, C. A., & Klein, G. (2002). E-cadherin-mediated interactions of thymic epithelial cells with CD103+ thymocytes lead to enhanced thymocyte cell proliferation. *Journal of cell science*, *115*(Pt 23), 4505–4515. https://doi.org/10.1242/jcs.00142

54. Lam, M., Mast, N., & Pikuleva, I. A. (2018). Drugs and Scaffold That Inhibit Cytochrome P450 27A1 In Vitro and In Vivo. *Molecular pharmacology*, *93*(2), 101–108. https://doi.org/10.1124/mol.117.110742
55. Lenschow, D. J., Su, G. H., Zuckerman, L. A., Nabavi, N., Jellis, C. L., Gray, G. S., Miller, J., & Bluestone, J. A. (1993). Expression and functional significance of an additional ligand for CTLA-4. *Proceedings of the National Academy of Sciences of the United States of America*, *90*(23), 11054–11058. https://doi.org/10.1073/pnas.90.23.11054
56. Lertkiatmongkol, P., Liao, D., Mei, H., Hu, Y., & Newman, P. J. (2016). Endothelial functions of platelet/endothelial cell adhesion molecule-1 (CD31). *Current opinion in hematology*, *23*(3), 253–259. https://doi.org/10.1097/MOH.0000000000000239
57. Lesbats, J., Brillac, A., Reisz, J. A., Mukherjee, P., Lhuissier, C., Fernández-Monreal, M., Dupuy, J. W., Sequeira, A., Tioli, G., De La Calle Arregui, C., Pinson, B., Wendisch, D., Rousseau, B., Efeyan, A., Sander, L. E., D'Alessandro, A., & Garaude, J. (2025). Macrophages recycle phagocytosed bacteria to fuel immunometabolic responses. *Nature*, 10.1038/s41586-025-08629-4. Advance online publication. https://doi.org/10.1038/s41586-025-08629-4
58. Li, L. T., Jiang, G., Chen, Q., & Zheng, J. N. (2015). Ki67 is a promising molecular target in the diagnosis of cancer (review). *Molecular medicine reports*, *11*(3), 1566–1572. https://doi.org/10.3892/mmr.2014.2914
59. Li, M., Yang, Y., Xiong, L., Jiang, P., Wang, J., & Li, C. (2023). Metabolism, metabolites, and macrophages in cancer. *Journal of hematology & oncology*, *16*(1), 80. https://doi.org/10.1186/s13045-023-01478-6
60. Lim, S. A., Wei, J., Nguyen, T. M., Shi, H., Su, W., Palacios, G., Dhungana, Y., Chapman, N. M., Long, L., Saravia, J., Vogel, P., & Chi, H. (2021). Lipid signalling enforces functional specialization of T_{reg} cells in tumours. *Nature*, *591*(7849), 306–311. https://doi.org/10.1038/s41586-021-03235-6
61. Liu, S. Y., Mulugeta, N., Dougan, S. K., & Qiang, L. (2023). In vitro flow cytometry assay to assess primary human and mouse macrophage phagocytosis of live cells. *STAR protocols*, *4*(2), 102240. Advance online publication. https://doi.org/10.1016/j.xpro.2023.102240
62. Llaverias, G., Danilo, C., Mercier, I., Daumer, K., Capozza, F., Williams, T. M., Sotgia, F., Lisanti, M. P., & Frank, P. G. (2011). Role of cholesterol in the development and progression of breast cancer. *The American journal of pathology*, *178*(1), 402–412. https://doi.org/10.1016/j.ajpath.2010.11.005
63. Martinez, F. O., & Gordon, S. (2014). The M1 and M2 paradigm of macrophage activation: time for reassessment. *F1000prime reports*, *6*, 13. https://doi.org/10.12703/P6-13
64. Mildner, A., Yona, S., & Jung, S. (2013). A close encounter of the third kind: monocyte-derived cells. *Advances in immunology*, *120*, 69–103. https://doi.org/10.1016/B978-0-12-417028-5.00003-X
65. Murray P. J. (2017). Macrophage Polarization. *Annual review of physiology*, *79*, 541–566. https://doi.org/10.1146/annurev-physiol-022516-034339
66. Nakaya, M., Xiao, Y., Zhou, X., Chang, J. H., Chang, M., Cheng, X., Blonska, M., Lin, X., & Sun, S. C. (2014). Inflammatory T cell responses rely on amino acid transporter ASCT2 facilitation of glutamine uptake and mTORC1 kinase activation. *Immunity*, *40*(5), 692–705. https://doi.org/10.1016/j.immuni.2014.04.007
67. Nelson, E. R., Wardell, S. E., Jasper, J. S., Park, S., Suchindran, S., Howe, M. K., Carver, N. J., Pillai, R. V., Sullivan, P. M., Sondhi, V., Umetani, M., Geradts, J., & McDonnell, D. P. (2013). 27-Hydroxycholesterol links hypercholesterolemia and breast cancer

pathophysiology. *Science (New York, N.Y.)*, *342*(6162), 1094–1098. https://doi.org/10.1126/science.1241908
68. Nicholson, D. W., Ali, A., Thornberry, N. A., Vaillancourt, J. P., Ding, C. K., Gallant, M., Gareau, Y., Griffin, P. R., Labelle, M., & Lazebnik, Y. A. (1995). Identification and inhibition of the ICE/CED-3 protease necessary for mammalian apoptosis. *Nature*, *376*(6535), 37–43. https://doi.org/10.1038/376037a0
69. Oishi, Y., & Manabe, I. (2018). Macrophages in inflammation, repair and regeneration. *International immunology*, *30*(11), 511–528. https://doi.org/10.1093/intimm/dxy054
70. Olsen, B. N., Schlesinger, P. H., Ory, D. S., & Baker, N. A. (2012). Side-chain oxysterols: from cells to membranes to molecules. *Biochimica et biophysica acta*, *1818*(2), 330–336. https://doi.org/10.1016/j.bbamem.2011.06.014
71. Pan Y, Yu Y, Wang X, Zhang T. Tumor-Associated Macrophages in Tumor Immunity. Front Immunol. 2020 Dec 3;11:583084. doi: 10.3389/fimmu.2020.583084. Erratum in: Front Immunol. 2021 Dec 10;12:775758. doi: 10.3389/fimmu.2021.775758. PMID: 33365025; PMCID: PMC7751482.
72. Pelka, K., Hofree, M., Chen, J. H., Sarkizova, S., Pirl, J. D., Jorgji, V., Bejnood, A., Dionne, D., Ge, W. H., Xu, K. H., Chao, S. X., Zollinger, D. R., Lieb, D. J., Reeves, J. W., Fuhrman, C. A., Hoang, M. L., Delorey, T., Nguyen, L. T., Waldman, J., Klapholz, M., … Hacohen, N. (2021). Spatially organized multicellular immune hubs in human colorectal cancer. *Cell*, *184*(18), 4734–4752.e20. https://doi.org/10.1016/j.cell.2021.08.003
73. Pelton, K., Freeman, M. R., & Solomon, K. R. (2012). Cholesterol and prostate cancer. *Current opinion in pharmacology*, *12*(6), 751–759. https://doi.org/10.1016/j.coph.2012.07.006
74. Philip, M., & Schietinger, A. (2022). $CD8^+$ T cell differentiation and dysfunction in cancer. *Nature reviews. Immunology*, *22*(4), 209–223. https://doi.org/10.1038/s41577-021-00574-3
75. Qian, B. Z., & Pollard, J. W. (2010). Macrophage diversity enhances tumor progression and metastasis. *Cell*, *141*(1), 39–51. https://doi.org/10.1016/j.cell.2010.03.014
76. Ravnskov, U., McCully, K. S., & Rosch, P. J. (2012). The statin-low cholesterol-cancer conundrum. *QJM : monthly journal of the Association of Physicians*, *105*(4), 383–388. https://doi.org/10.1093/qjmed/hcr243
77. Reina-Campos, M., Scharping, N. E., & Goldrath, A. W. (2021). $CD8^+$ T cell metabolism in infection and cancer. *Nature reviews. Immunology*, *21*(11), 718–738. https://doi.org/10.1038/s41577-021-00537-8
78. Revilla, G., Pons, M. P., Baila-Rueda, L., García-León, A., Santos, D., Cenarro, A., Magalhaes, M., Blanco, R. M., Moral, A., Ignacio Pérez, J., Sabé, G., González, C., Fuste, V., Lerma, E., Faria, M. D. S., de Leiva, A., Corcoy, R., Carles Escolà-Gil, J., & Mato, E. (2019). Cholesterol and 27-hydroxycholesterol promote thyroid carcinoma aggressiveness. *Scientific reports*, *9*(1), 10260. https://doi.org/10.1038/s41598-019-46727-2
79. Rossin, D., Dias, I. H. K., Solej, M., Milic, I., Pitt, A. R., Iaia, N., Scoppapietra, L., Devitt, A., Nano, M., Degiuli, M., Volante, M., Caccia, C., Leoni, V., Griffiths, H. R., Spickett, C. M., Poli, G., & Biasi, F. (2019). Increased production of 27-hydroxycholesterol in human colorectal cancer advanced stage: Possible contribution to cancer cell survival and infiltration. *Free radical biology & medicine*, *136*, 35–44. https://doi.org/10.1016/j.freeradbiomed.2019.03.020
80. Ryan, D. G., & O'Neill, L. A. J. (2020). Krebs Cycle Reborn in Macrophage Immunometabolism. *Annual review of immunology*, *38*, 289–313. https://doi.org/10.1146/annurev-immunol-081619-104850

81. Safwan-Zaiter, H., Wagner, N., & Wagner, K. D. (2022). P16INK4A-More Than a Senescence Marker. *Life (Basel, Switzerland)*, *12*(9), 1332. https://doi.org/10.3390/life12091332
82. Saha P, Ettel P, Weichhart T. Leveraging macrophage metabolism for anticancer therapy: opportunities and pitfalls. Trends Pharmacol Sci. 2024 Apr;45(4):335-349. doi: 10.1016/j.tips.2024.02.005. Epub 2024 Mar 17. PMID: 38494408.
83. Sahasrabuddhe V, Ghosh HS. Cx3Cr1-Cre induction leads to microglial activation and IFN-1 signaling caused by DNA damage in early postnatal brain. Cell Rep. 2022 Jan 18;38(3):110252. doi: 10.1016/j.celrep.2021.110252. PMID: 35045285.
84. Salmaninejad, A., Valilou, S. F., Soltani, A., Ahmadi, S., Abarghan, Y. J., Rosengren, R. J., & Sahebkar, A. (2019). Tumor-associated macrophages: role in cancer development and therapeutic implications. *Cellular oncology (Dordrecht, Netherlands)*, *42*(5), 591–608. https://doi.org/10.1007/s13402-019-00453-z
85. Saraiva, M., & O'Garra, A. (2010). The regulation of IL-10 production by immune cells. *Nature reviews. Immunology*, *10*(3), 170–181. https://doi.org/10.1038/nri2711
86. Schroepfer G. J., Jr (2000). Oxysterols: modulators of cholesterol metabolism and other processes. *Physiological reviews*, *80*(1), 361–554. https://doi.org/10.1152/physrev.2000.80.1.361
87. Schrörs, B., Hos, B. J., Yildiz, I. G., Löwer, M., Lang, F., Holtsträter, C., Becker, J., Vormehr, M., Sahin, U., Ossendorp, F., & Diken, M. (2023). MC38 colorectal tumor cell lines from two different sources display substantial differences in transcriptome, mutanome and neoantigen expression. *Frontiers in immunology*, *14*, 1102282. https://doi.org/10.3389/fimmu.2023.1102282
88. Scodeller, P., Simón-Gracia, L., Kopanchuk, S., Tobi, A., Kilk, K., Säälik, P., Kurm, K., Squadrito, M. L., Kotamraju, V. R., Rinken, A., De Palma, M., Ruoslahti, E., & Teesalu, T. (2017). Precision Targeting of Tumor Macrophages with a CD206 Binding Peptide. *Scientific reports*, *7*(1), 14655. https://doi.org/10.1038/s41598-017-14709-x
89. Seyfried T. N. (2015). Cancer as a mitochondrial metabolic disease. *Frontiers in cell and developmental biology*, *3*, 43. https://doi.org/10.3389/fcell.2015.00043
90. Sharma, P., Siddiqui, B. A., Anandhan, S., Yadav, S. S., Subudhi, S. K., Gao, J., Goswami, S., & Allison, J. P. (2021). The Next Decade of Immune Checkpoint Therapy. *Cancer discovery*, *11*(4), 838–857. https://doi.org/10.1158/2159-8290.CD-20-1680
91. Shi, J., Hua, L., Harmer, D., Li, P., & Ren, G. (2018). Cre Driver Mice Targeting Macrophages. *Methods in molecular biology (Clifton, N.J.)*, *1784*, 263–275. https://doi.org/10.1007/978-1-4939-7837-3_24
92. Singer, K., Cheng, W. C., Kreutz, M., Ho, P. C., & Siska, P. J. (2018). Immunometabolism in cancer at a glance. *Disease models & mechanisms*, *11*(8), dmm034272. https://doi.org/10.1242/dmm.034272
93. Singh, S., Anshita, D., & Ravichandiran, V. (2021). MCP-1: Function, regulation, and involvement in disease. *International immunopharmacology*, *101*(Pt B), 107598. https://doi.org/10.1016/j.intimp.2021.107598
94. Slominski, A. T., Kim, T. K., Janjetovic, Z., Slominski, R. M., Li, W., Jetten, A. M., Indra, A. K., Mason, R. S., & Tuckey, R. C. (2024). Biological Effects of CYP11A1-Derived Vitamin D and Lumisterol Metabolites in the Skin. *The Journal of investigative dermatology*, *144*(10), 2145–2161. https://doi.org/10.1016/j.jid.2024.04.022
95. Su, Y. R., Linton, M. F., & Fazio, S. (2002). Rapid quantification of murine ABC mRNAs by real time reverse transcriptase-polymerase chain reaction. *Journal of lipid research*, *43*(12), 2180–2187. https://doi.org/10.1194/jlr.d200020-jlr200
96. Sung, H., Ferlay, J., Siegel, R. L., Laversanne, M., Soerjomataram, I., Jemal, A., & Bray, F. (2021). Global Cancer Statistics 2020: GLOBOCAN Estimates of Incidence and

Mortality Worldwide for 36 Cancers in 185 Countries. CA: a cancer journal for clinicians, 71(3), 209–249. https://doi.org/10.3322/caac.21660
97. Svensson, S., Ostberg, T., Jacobsson, M., Norström, C., Stefansson, K., Hallén, D., Johansson, I. C., Zachrisson, K., Ogg, D., & Jendeberg, L. (2003). Crystal structure of the heterodimeric complex of LXRalpha and RXRbeta ligand-binding domains in a fully agonistic conformation. *The EMBO journal*, *22*(18), 4625–4633. https://doi.org/10.1093/emboj/cdg456
98. Tian, W., Pang, W., Ge, Y., He, X., Wang, D., Li, X., Hou, H., Zhou, D., Feng, S., Chen, Z., & Yang, Y. (2018). Hepatocyte-generated 27-hydroxycholesterol promotes the growth of melanoma by activation of estrogen receptor alpha. *Journal of cellular biochemistry*, *119*(3), 2929–2938. https://doi.org/10.1002/jcb.26498
99. Fritsch, S. D., Sukhbaatar, N., Gonzales, K., Sahu, A., Tran, L., Vogel, A., Mazic, M., Wilson, J. L., Forisch, S., Mayr, H., Oberle, R., Weiszmann, J., Brenner, M., Vanhoutte, R., Hofmann, M., Pirnes-Karhu, S., Magnes, C., Kühnast, T., Weckwerth, W., Bock, C., … Weichhart, T. (2023). Metabolic support by macrophages sustains colonic epithelial homeostasis. Cell metabolism, 35(11), 1931–1943.e8. https://doi.org/10.1016/j.cmet.2023.09.010
100. Upadhyay A. (2020). Cancer: An unknown territory; rethinking before going ahead. *Genes & diseases*, *8*(5), 655–661. https://doi.org/10.1016/j.gendis.2020.09.002
101. van Gulijk, M., van Krimpen, A., Schetters, S., Eterman, M., van Elsas, M., Mankor, J., Klaase, L., de Bruijn, M., van Nimwegen, M., van Tienhoven, T., van Ijcken, W., Boon, L., van der Schoot, J., Verdoes, M., Scheeren, F., van der Burg, S. H., Lambrecht, B. N., Stadhouders, R., Dammeijer, F., Aerts, J., … van Hall, T. (2023). PD-L1 checkpoint blockade promotes regulatory T cell activity that underlies therapy resistance. *Science immunology*, *8*(83), eabn6173. https://doi.org/10.1126/sciimmunol.abn6173
102. Vaz, F. M., & Ferdinandusse, S. (2017). Bile acid analysis in human disorders of bile acid biosynthesis. *Molecular aspects of medicine*, *56*, 10–24. https://doi.org/10.1016/j.mam.2017.03.003
103. Vercellino, I., & Sazanov, L. A. (2022). The assembly, regulation and function of the mitochondrial respiratory chain. *Nature reviews. Molecular cell biology*, *23*(2), 141–161. https://doi.org/10.1038/s41580-021-00415-0
104. Vo, D.-K., Nguyen, L., & Maeng, H.-J. (2024). Impact of 1α,25-dihydroxyvitamin D3 on biodistribution and pharmacokinetics of L-carnitine and creatinine, organic cation/carnitine transporter 2 and organic cation transporter 2 biomarkers. Journal of Pharmaceutical Investigation, 54. https://doi.org/10.1007/s40005-023-00659-2
105. Wang, C., Ma, C., Gong, L., Guo, Y., Fu, K., Zhang, Y., Zhou, H., & Li, Y. (2021). Macrophage Polarization and Its Role in Liver Disease. *Frontiers in immunology*, *12*, 803037. https://doi.org/10.3389/fimmu.2021.803037
106. Wang, Z., Chen, C., Su, Y., & Ke, N. (2023). Function and characteristics of TIM-4 in immune regulation and disease (Review). *International journal of molecular medicine*, *51*(2), 10. https://doi.org/10.3892/ijmm.2022.5213
107. Warburg, O., Posener, K., & Negelein, E. (1924). Über den Stoffwechsel der Tumoren [On the metabolism of tumors]. *Biochemische Zeitschrift, 152*, 319–344.
108. Wei, Q., Deng, Y., Yang, Q., Zhan, A., & Wang, L. (2023). The markers to delineate different phenotypes of macrophages related to metabolic disorders. *Frontiers in immunology*, *14*, 1084636. https://doi.org/10.3389/fimmu.2023.1084636
109. Willis, B. C., Johnson, G., Wang, J., & Cohen, C. (2015). SOX10: a useful marker for identifying metastatic melanoma in sentinel lymph nodes. *Applied*

immunohistochemistry & molecular morphology: AIMM, *23*(2), 109–112. https://doi.org/10.1097/PAI.0000000000000097

110. Wu, H., Gower, R. M., Wang, H., Perrard, X. Y., Ma, R., Bullard, D. C., Burns, A. R., Paul, A., Smith, C. W., Simon, S. I., & Ballantyne, C. M. (2009). Functional role of CD11c+ monocytes in atherogenesis associated with hypercholesterolemia. *Circulation*, *119*(20), 2708–2717. https://doi.org/10.1161/CIRCULATIONAHA.108.823740

111. Xue, J., Schmidt, S. V., Sander, J., Draffehn, A., Krebs, W., Quester, I., De Nardo, D., Gohel, T. D., Emde, M., Schmidleithner, L., Ganesan, H., Nino-Castro, A., Mallmann, M. R., Labzin, L., Theis, H., Kraut, M., Beyer, M., Latz, E., Freeman, T. C., Ulas, T., … Schultze, J. L. (2014). Transcriptome-based network analysis reveals a spectrum model of human macrophage activation. *Immunity*, *40*(2), 274–288. https://doi.org/10.1016/j.immuni.2014.01.006

112. Yan, C., Zheng, L., Jiang, S., Yang, H., Guo, J., Jiang, L. Y., Li, T., Zhang, H., Bai, Y., Lou, Y., Zhang, Q., Liang, T., Schamel, W., Wang, H., Yang, W., Wang, G., Zhu, Z. J., Song, B. L., & Xu, C. (2023). Exhaustion-associated cholesterol deficiency dampens the cytotoxic arm of antitumor immunity. *Cancer cell*, *41*(7), 1276–1293.e11. https://doi.org/10.1016/j.ccell.2023.04.016

113. Yona, S., Kim, K. W., Wolf, Y., Mildner, A., Varol, D., Breker, M., Strauss-Ayali, D., Viukov, S., Guilliams, M., Misharin, A., Hume, D. A., Perlman, H., Malissen, B., Zelzer, E., & Jung, S. (2013). Fate mapping reveals origins and dynamics of monocytes and tissue macrophages under homeostasis. *Immunity*, *38*(1), 79–91. https://doi.org/10.1016/j.immuni.2012.12.001

114. Yunna, C., Mengru, H., Lei, W., & Weidong, C. (2020). Macrophage M1/M2 polarization. *European journal of pharmacology*, *877*, 173090. https://doi.org/10.1016/j.ejphar.2020.173090

115. Zordan, P., Rigamonti, E., Freudenberg, K., Conti, V., Azzoni, E., Rovere-Querini, P., & Brunelli, S. (2014). Macrophages commit postnatal endothelium-derived progenitors to angiogenesis and restrict endothelial to mesenchymal transition during muscle regeneration. *Cell death & disease*, *5*(1), e1031. https://doi.org/10.1038/cddis.2013.558

7. Supplementary Material

Primary antibodies used in this study for FACS				
Target	**Fluorophore**	**Company**	**Catalog Number**	**Catalog Number**
B220 (CD45R)	APC	Invitrogen	17-0452-82	1:100
B220 (CD45R)	eF450	Invitrogen	48-0452-82	1:100
CD103	AF700	Invitrogen	56-1031-82	1:100
CD103	PE/Cy7	BioLegend	110909	1:100
CD11b	APC	BioLegend	101212	1:100
CD11b	eF450	Invitrogen	48-0112-82	1:100
CD11c	PE/Cy7	Invitrogen	25-0114-82	1:100
CD196/Siglec-1	BV605	BioLegend	142413	1:100
CD206	AF700	BioLegend	141734	1:100
CD206	PE	BioLegend	162504	1:100
CD279 (PD-1)	BV605	BD Biosciences	563059	1:100
CD36	AF488	BioLegend	102608	1:100
CD3e	AF700	BioLegend	152316	1:100
CD4	APC	BioLegend	100516	1:100
CD4	BV605	BioLegend	100451	1:100
CD40	PE	BioLegend	124609	1:100
CD45.2	PerCP-Cy5.5	Invitrogen	45-0454-82	1:100
CD86	BV650	BioLegend	105036	1:100
CD8a	BV650	BD Biosciences	563234	1:100
F4/80	APC	BioLegend	157306	1:100
F4/80	FITC	Miltenyi Biotec	130-117-509	1:100
F4/80	BV605	BioLegend	123133	1:100
FVD (Dead Cells)	eF780	Thermo Fisher	65-0865-14	1:100
GzmB	eF450	Thermo Fisher	48-8898-82	1:100
I-A/I-E (MHCII)	BV510	BioLegend	107635	1:100
IFN-γ	PE	eBioscience	12-7311-82	1:100
Ly6C	AF700	BioLegend	128024	1:100
Ly6C	PE	BioLegend	128007	1:100
Ly6G	PE	BioLegend	164503	1:100
Ly6G	PerCP-Cy5.5	BioLegend	127615	1:100

MHCII (1-A/1-E)	BV605	BD Biosciences	743872	1:100
NK1.1	BV510	BioLegend	108737	1:100
TIM-4	PerCP-eFluor 710	Invitrogen	46-5866-82	1:100
TNF-α	PE	Thermo Fisher	12-7423-41	1:100

Tabel 1. Antibodies used in this study for FACS

This table presents the primary antibodies with conjugated fluorophores used in this study for FACS based assays, listed in alphabetical order. The table includes the target of the antibody, the conjugated fluorophore, the manufacturer, the catalog number assigned by the manufacturer, and the dilution used in the experiments

Primary antibodies used in this study for histology				
Name/Target	**Host**	**Manufacturer**	**Catalog Number**	**Dilution**
CD206	Goat	Invitrogen	PA5-46994	1:200 (IF)
CD31	Rat	Dianova	DIA-310	1:100 (IF)
CD31	Rabbit	CST	77699	1:100 (IF)
CD31	Rabbit	CST	77699	1:100 (IF FFPE)
CD45	Rabbit	CST	70257	1:100 (IF FFPE)
CD68	Mouse	Invitrogen	14-0688-82	1:100 (IF)
CD8	Rabbit	Bioss	bs-0648R	1:200 (IF)
CDKN2A/p19ARF	Rabbit	Abcam	Ab80	1:100 (ICH)
Cleaved Caspase 3	Rabbit	CST	9664	1:200 (IF)
CYP27A1	Rabbit	Abcam	ab126785	1:50 (IF)
F4/80	Rat	BioLegend	123102	1:100 (IF)
Ki67	Rat	Invitrogen	14-5698-82	1:100 (IF)
Mac2	Goat	R&D Systems	AF1197	1:100 (IF)
Sox10	Rabbit	Abcam	ab180862	1:100 (IF FFPE)
Sox10	Goat	Invitrogen	PA5-37890	1:500 (IF)

Tabel 2. Antibodies used in this study for immunofluorescence and immunohistochemistry

This table presents the primary antibodies used in this study for immunofluorescence and immunohistochemistry stainings, listed in alphabetical order. The table includes the target of the

antibody, the host animal in which it was produced, the manufacturer, the catalog number assigned by the manufacturer, and the dilution used in the experiments.

Secondary antibodies and reagents-based staining used in this study				
Name/Target	**Host**	**Manufacturer**	**Catalog Number**	**Dilution**
Anti-Goat IgG H&L (Alexa Fluor® 488)	Donkey	Invitrogen	A32814	1:500
Anti-Goat IgG H&L (Alexa Fluor® 555)	Donkey	Invitrogen	A32816	1:500
Anti-Goat IgG H&L (Alexa Fluor® 647)	Donkey	Invitrogen	A32849	1:500
Anti-Puromycin Alexa Fluor® 488	Mouse	Merck	MABE343-AF488	1:1000
Anti-Rabbit IgG Antibody (H+L), Biotinylated	Horse	Vector Labs	BA-1100	1:500
Anti-Rabbit IgG H&L (Alexa Fluor® 488)	Donkey	Invitrogen	A32790	1:500
Anti-Rabbit IgG H&L (Alexa Fluor® 647)	Donkey	Invitrogen	A32795	1:500
Anti-Rabbit IgG H&L (Alexa Fluor® 555)	Donkey	Invitrogen	A31572	1:500
Anti-Rabbit IgG H&L (Alexa Fluor® 647)	Donkey	Invitrogen	A32795	1:500
Anti-Rat IgG H&L (Alexa Fluor® 488)	Rabbit	Invitrogen	A21210	1:500
Anti-Rat IgG H&L (Alexa Fluor® 555)	Donkey	Abcam	ab150154	1:500
Anti-Rat IgG H&L (DyLight® 650)	Donkey	Invitrogen	SA5-10029	1:500
BODIPY™ 493/503		Thermo Fisher	D3922	1:100
DAPI HCl, 4′,6-Diamidino-2-phenylindole dihydrochloride		Merck	D9542	1:500

Tabel 3. Secondary antibodies and fluorescent dyes used in this

This table presents the secondary antibodies with conjugated fluorophores and fluorescent

dyes used in this study, listed in alphabetical order. The table includes the target of the antibody, the host animal in which it was produced, the manufacturer, the catalog number assigned by the manufacturer, and the dilution used in the experiments.

Primers/Oligos used in this study

Target/Name	Direction	Sequence	TM (in °C)
ATP-binding cassette sub-family A member 1	Forward	GGACATGCACAAGGTCCTGA	59,4
	Reverse	CAGAAAATCCTGGAGCTTCAAA	56,5
ATP-binding cassette sub-family G member 8	Forward	CCTTCCTCAGCATCATGCG	58,8
	Reverse	CCGATCCCAATGTGCGA	55,2
Angiopoietin-like 4	Forward	GATGGCTCAGTGGACTTCAACC	68
	Reverse	TGCTATGCACCTTCTCCAGACC	69
Apolipoprotein E	Forward	GAACCGCTTCTGGGATTACCTG	62,1
	Reverse	GCCTTTACTTCCGTCATAGTGTC	60,7
Arginase-1	Forward	AGG TCC CCG TGG TCT CTC ACG	74
	Reverse	AAG GAC AGC CTC GAG GAG GGG T	75
β-actin	Forward	TTG CAC ATG CCG CAG CCG TT	74
	Reverse	CAC ACC CGC CAC CAG TTC GC	75
Cytochrome P450 Family 27 Subfamily A Member 1	Forward	GGC TAC CTG CAC TTC CT	55,2
	Reverse	CTG GAT CTC TGG GCT CTT TG	59,4
Interleukin 10	Forward	CCC CAG GCA GAG AAG CAT GGC	65,68
	Reverse	GGG GAG AAA TCG ATG ACA GCG CC	66
Inducible Nitric Oxide Synthase	Forward	CGG GCA TCT GGT AGC CAG CG	74
	Reverse	TGG CAA CAT CAG GTC GGC CAT	72

Macrophage mannose receptor	Forward	ACA TGC CAG GAC GAA AGG CGG	63,73
	Reverse	TTG TGG GCT CTG GTG GGC GA	63,45
Liver X Receptor Beta	Forward	AGATGGATGCCTTCATGCGG	56,5
	Reverse	TCCGAATCTGCTCCTCAGAGA	58,8
Liver X Receptor Alpha	Forward	AAACAGCTCCCTGGCTTCCT	59,4
	Reverse	GTACCTCCGTGACGTCTCCA	59,4
Tumor Necrosis Factor Alpha	Forward	GCA GCC TTG TCC CTT GAA GA	68
	Reverse	ACG TCG TAG CAA ACC ACC AA	67

Tabel 4. Primers/Oligos used in this study

This table presents the primers/oligos used in this study, listed in alphabetical order. The table includes the target gene, if it's the forward or reverse primer, the sequence and the melting temperature (TM) in °C.